CHAPTER 12

Efficiency of CAT and L-SIGN as alternative or co-receptors for SARS-CoV-2 Spike Protein

Efficiency of CAT and L-SIGN as alternative or co-receptors for SARS-CoV-2 Spike Protein

12.1. Abstract:

The COVID-19 disease, which is caused by SARS-CoV-2, has been spreading rapidly over the world since December 2019 and has become a serious threat to human health. According to reports, SARS-CoV-2 infection has an impact on several human tissues, including the kidney, gastrointestinal system, and lung. The Spike (S) protein from SARS-CoV-2 has been found to primarily bind ACE2. Since the lungs are the organ that COVID-19 is most likely to infect, the comparatively low expression of this recognized receptor suggests that there may be alternative co-receptors or alternative SARS-CoV-2 receptors that cooperate with ACE2. Recently, many candidate receptors of SARS-CoV-2 other than ACE2 were reported to be specifically and highly expressed in SARS-CoV-2 affected tissues. Among these receptors, the binding affinity of CAT and L-SIGN to the S protein has been reported to be higher in one of the recent studies. So, it will be significant to understand the binding interactions between these potential receptors and the RBD region of the S protein. In this study, we compared the interaction profile of the RBD of the S protein of SARS-CoV-2 with CAT and L-SIGN receptors. From the MD simulation study, the S protein employs special techniques to have stable interactions with the CAT and L-SIGN receptors (ΔG_{bind} = -39.49 kcal/mol and -35.11 kcal/mol, respectively). SARS-CoV-2 may result in greater virulence as a result of the S protein-CAT complex's stability and the greater affinity of spike protein for the CAT receptor.

12.2. Introduction:

The coronavirus disease that has been a threat to human health and society was caused by the severe acute respiratory syndrome coronavirus 2 (SARS-CoV-2) [1]. According to the phylogenetic analysis of the whole viral genome consisting of 29,903 nucleotides, the virus was found to be most closely related to a group of SARS-like coronaviruses that had previously been detected in bats in China with 89.1% nucleotide similarity [2]. More than 6,873,799 fatalities had been documented globally as of May 2023, and the figure continues to rise. Fever, cough and myalgia or fatigue were found to be the common symptoms of COVID-19 illness and sputum production, headache, hemoptysis, and diarrhea were found to be lesser common symptoms. Complications included acute respiratory distress syndrome, RNAaemia, acute cardiac injury and secondary infection [3]. Infectivity based natural selection was discovered as the mechanism for SARS-CoV-2 evolution and transmission. Studies suggest that the RBD co-mutations will have high chances to grow into dominating variants which may be the main

cause for the transition of CoV [4-7]. In order to develop possible antiviral drugs against this virus, it is imperative that the path ways of SARS-CoV-2 entry into the host be thoroughly studied [8]. The entry of the SARS-CoV-2 into the host cell is said to be dependent on the spike (S) protein and binding to the major functional receptor ACE2 [9]. A receptor-binding domain (RBD) is a key part of a virus located on the spike domain that allows it to dock to body receptors to gain entry into cells and lead to infection. RBD is a short immunogenic fragment from a virus and why studies focus mainly on the RBD instead of the whole spike is that it binds to a specific receptor sequence which is required to interact with the endogenous receptors to facilitate membrane fusion and delivery to the cytoplasm. Moreover, RBD is also treated as the primary target in the prevention and treatment of viral infections, including severe acute respiratory syndrome corona virus 2 (SARS-CoV-2), the virus that causes COVID-19. Another reason why RBD is considered a core for study is because of its confirmation. The SARS-CoV-2 RBD has a twisted 5-stranded antiparallel beta-sheet with short connecting helices and loops. In the core, between the β4-7 strands, there is an additional extended insertion containing short β5 6 strands. This extension is where the receptor-binding motif (RBM) is, which contains the contacting residues that enable it to bind to ACE2. The binding of the RBD on the spike domain is a critical step that allows coronaviruses to bind to target body receptors (such as ACE2 on respiratory epithelial cells) and enter cells to cause infection. The RBD is therefore an important target for neutralizing antibodies [10-15]. Studies mainly involved the Receptor binding domain (RBD) of spike protein, the accessibility of RBD to ACE2, its key residues for stronger binding to ACE2 which is the origin of the stronger binding, and its potential sites for drug and antibody design were explored [16-18]. However, there are limitations in considering exclusively the RBD region as the mutations are found to appear in the other regions of the spike protein which either strengthen the interaction between the spike and ACE2 receptor or weaken the interactions. So, considering only the RBD region may limit the study of the effect of the other mutations occurring outside the RBD region. Moreover, the receptors and co receptors are found to bind to a few residues present outside the receptor binding domain. So, considering the RBD only may not give us accurate results in some cases [19, 20]. According to the previous studies, it has been determined that the ACE2 receptor, which works as a primary receptor for virus entry is primarily expressed in lungs, liver cholangiocyte, colon colonocytes, esophagus keratinocytes, ileum ECs, rectum ECs, stomach epithelial cells, and kidney proximal tubules [21]. Moreover, it was also found the ex pression of the primary receptor of SARS-CoV-2 that is ACE2 was found to be relatively low in those organs, which may suggest that other alternative receptors like CAT and L SIGN are involved in facilitating the entry of SARS-CoV-2 inside the host cell [22, 23]. CAT is a catalase that is mainly expressed by the protein class: Cancer-related genes, Disease-related genes, Enzymes, FDA-approved drug targets,

Human disease-related genes, Metabolic proteins, and Plas ma proteins. Most importantly, CAT is a key antioxidant enzyme, that is specifically expressed in the lungs, kidney, and intestine which are the most affected tissues during COVID-19. According to the Human Protein Atlas, overexpression of CAT has been reported to reduce renal oxidative stress, prevent hypertension and show a correlation with ACE2 expression. Intriguingly, ACE2 deficiency can increase NADPH-mediated oxidative stress in the kidney, suggesting a possible link with CAT. Furthermore, a study by Dongjie Guo and his group suggested that protein-protein interaction simulations revealed that CAT could bind to S protein with a higher binding affinity than ACE2 [24]. Also, there is strong evidence that the S protein binding protein associated with SARS-CoV-2 and CAT interact. In addition, their results of intracellular localization demonstrated the presence of CAT protein and ACE2 in both the extracellular area and cell membrane. Therefore, they have concluded that the binding efficiency of ACE2 is significantly influenced by CAT, which in turn affects COVID 19 susceptibility [25]. Moreover, studies also suggested that L-SIGN could also bind to SARS-CoV-2 S protein and act as an alternative or co-receptor of spike. Immunofluorescence staining of human tissues revealed prominent expression of CD209L(L-SIGN) in the lung and kidney epithelium and endothelium, the most infected organ during COVID-19. Multiple biochemical as says using a purified recombinant SARS-CoV-2 spike receptor binding domain (S-RBD) or S1 encompassing both NTB and RBD and ectopically expressed L-SIGN, revealed that CD209L interact with S-RBD. L-SIGN contains two N glycosylation sequons, at sites N92 and N361, but only site N92 is occupied. Removal of the N-glycosylation at this site enhances the binding of S-RBD with L-SIGN. L-SIGN also interacts with ACE2, suggesting a role for heterodimerization of L-SIGN and ACE2 in SARS-CoV-2 entry and infection in cell types where both are present. Studies suggest that L-SIGN serves as alternative receptors for SARS-CoV-2 in disease-relevant cell types, including the vascular system. This property is particularly important in tissues where ACE2 has low expression or is absent and may have implications for antiviral drug development. Moreover, the loss of L-SIGN in mice significantly reduced SARS-CoV infection, further emphasizing the critical role of L-SIGN in SARS-CoV infection. Furthermore, L-SIGN both appear to have higher affinities with SARS-CoV-2 S protein even than ACE2, suggesting that these two proteins may function as the alternative receptors independent of ACE2 [26, 27]. Recent studies suggest that a number of ACE2 interacting proteins that were specifically produced in infected tissues and exhibited high affinity for the S protein may function as ACE2 co-receptors to effectively bind to the S protein and promote efficient entry of SARS-CoV-2 into the host cells. On the other hand, future studies focus on other new receptors in addition to the ACE2 co-receptor. Many human cellular glycoprotein that can serve as an alternative receptor for SARS-CoV-2 apart from ACE2 has been report ed in recent studies [24]. Sequencing of the human lung

cDNA inserts showed that each of the cloned cell lines contained cDNA that encoded human, L-SIGN (also called CD209L). The findings of that study indicate that ACE2 and L-SIGN may be involved in virus infection and pathogenesis by the large S glycoprotein of SARS-CoV-2 [28, 29]. In recent studies, many candidate receptors for SARS CoV-2 have been identified which were particularly and abundantly expressed in tissues that have been exposed to the virus. Dongjie Guo and his group in their recent study reported five potential receptors, namely CAT, L-SIGN, DC-SIGN, MME and AGTR2. These receptors not only showed distinct expression levels in the lungs and other organs infected with COVID-19 but also had higher binding affinities with S protein than ACE2 [24]. These findings led them to hypothesize that such receptors would serve as co- or alternate receptors for SARS-CoV-2, and they anticipated that the binding hot spots at the receptor-S protein binding inter faces could serve as COVID-19 therapeutic targets. In this study, we compared the interaction profile of the Receptor Binding Domain of spike protein (RBD of S protein) with the CAT and L-SIGN receptors. We observed through the MD simulation analysis that the S protein employs specific methods to have a stable interaction with the CAT and L-SIGN receptors. The binding affinity of the S protein bound to the CAT receptor complex was found to be indeed high (ΔG_{bind} = -39.49 kcal/mol) in comparison with the S protein bound to L-SIGN receptor complex (ΔG_{bind} = -37.20 kcal/mol).

12.3. Materials and Method:

12.3.1. Online resources

The 3D structure of the RBD of the S protein was retrieved from the RBD of the S protein-ACE2 complex structure (PDB Id: 6lzg) available in the RCSB-PDB [30] using the CHIMERA package [31]. The glycosylation is not considered in the modelling of the structure of spike protein. The 3-D structure of the CAT receptor was not available in the RCSB. So, to predict the 3-D structure of CAT, the amino acid sequence was obtained from Ensemble (https://asia.ensembl.org/index.html).

12.3.2. Protein structures prediction

The 3-D structure of the L-SIGN receptor was down loaded from the RCSB-PDB with PDB Id 1XPH and that for the CAT receptor was predicted by submitting its amino acid sequence in the online server I-TASSER [32]. For the CAT receptor, five models were derived using I-TASSER, and the model with the highest C-score was selected as the best one and used as the basis for the subsequent study.

12.3.3. Preparation of SARS-CoV-2 RBD of S Protein-Receptor complexes

The two complexes (S protein-L-SIGN and S protein CAT) were prepared using the HADDOCK online docking server [33] and the 3D structures of both complexes are shown in **Figure 12.1.**

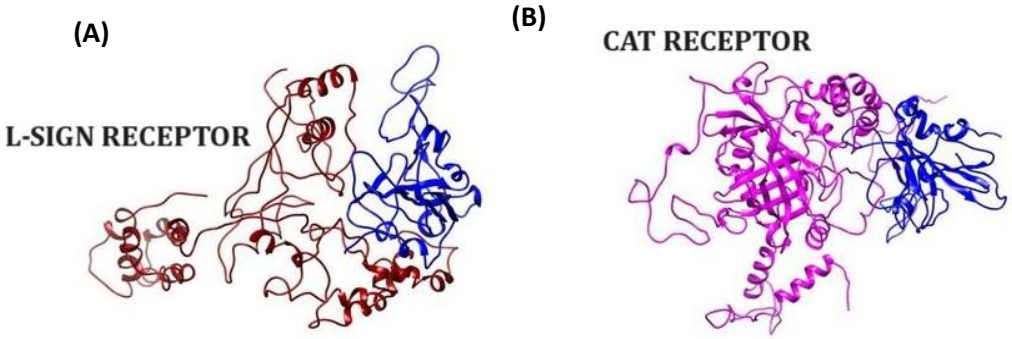

Figure 12.1. *The 3-D structure of* ***(A)*** *SARS-CoV-2 spike receptor-binding domain bound with L-SIGN (S protein-L-SIGN) and* ***(B)*** *SARS-CoV-2 spike receptor-binding domain bound with CAT (S protein-CAT).*

12.3.4. Molecular Dynamics Simulations

Energy minimization was carried out for the two complex systems (SARS-CoV-2 S-L-SIGN complex and SARS-CoV 2 S-CAT complex) in two steps, first is the steepest descents method, followed by conjugate gradient minimization. Then, we performed the MD simulation using the AMBER ff14SB force field and AMBER software package [34-36] for the two complex systems. Appropriate numbers of counter ions were added to the two complex systems to ensure their overall neutrality. With the TIP3P water model [37, 38], the two complex systems were solvated using an explicit solvent and a solvent buffer of 10 in all directions. In the first step of minimization, the S receptor-binding domain and the two receptors (CAT and L-SIGN), the energy was minimized for all the water molecules and counterions for 10000 steps of steepest descents (SD) followed by 10000 steps of the con jugate gradient (CG). The second step in minimization was carried out in order to eliminate the conflicting contacts and was performed on the entire complex system. This process was continued for 8000 steps for CG minimization and 12000 steps for SD minimization. After that, both complex systems were heated gradually under constant volume (NVT) conditions from 0 to 300 K, applying harmonic restraints to the solute atoms with a force constant of 10 kcal/mol/2, and performing three rounds of 3000 ps equilibration with a force constant of 5.0 kcal/mol/2. The NPT ensemble was then used to run 100 ns MD simulations without any constraints. We limited the direct space sum to treat the long-range electrostatic interactions using the Particle Mesh Ewald [39, 40] approach with a non-bonded cutoff of 12.0. All the bonds present in the system were constrained using the SHAKE algorithm [41]. Throughout the simulation, the Berendsen weak coupling algorithm [42] maintained a constant temperature and pressure (0.5 ps of heat

bath and 0.2 ps of pressure relaxation). The MD simulation time step was set at 2 fs, and the MD file was sampled every 10 ps.

12.3.5. Analysis of MD simulation trajectories

From the corresponding 100 ns MD trajectory files, the conformational dynamics and other important structural characteristics of both complexes (S protein-CAT and S pro tein-L-SIGN) were analysed. The following analysis: RMSD, RMSF and inter molecular hydrogen bond analysis were carried out using cpptraj module [43] of the AMBER software package and xmgrace plotting tool was used for generating the plots. From the highly populated clusters, the RMSD clustering algorithm was used to extract the lowest energy conformer of each complex (S protein-L-SIGN and S protein-CAT), which was then uploaded to the PDBsum server for analysis for residue-specific interactions, which are thought to be essential for understanding the nature of interactions. Schematic representations of the non-bonded interactions between amino acid residues at the interface of molecules in a multimer complex are gathered from the da tabase PDBsum server [44]. Snapshots of the SARS-CoV-2 L-SIGN-S Protein complex and SARS-CoV-2 CAT–S Protein structures at a discrete distance of separation (in Å) be tween their centre of mass are shown in **Figure 12.2 and 12.3**. A similar protocol was employed in our earlier studies on SARS-CoV-2 variants [45-47].

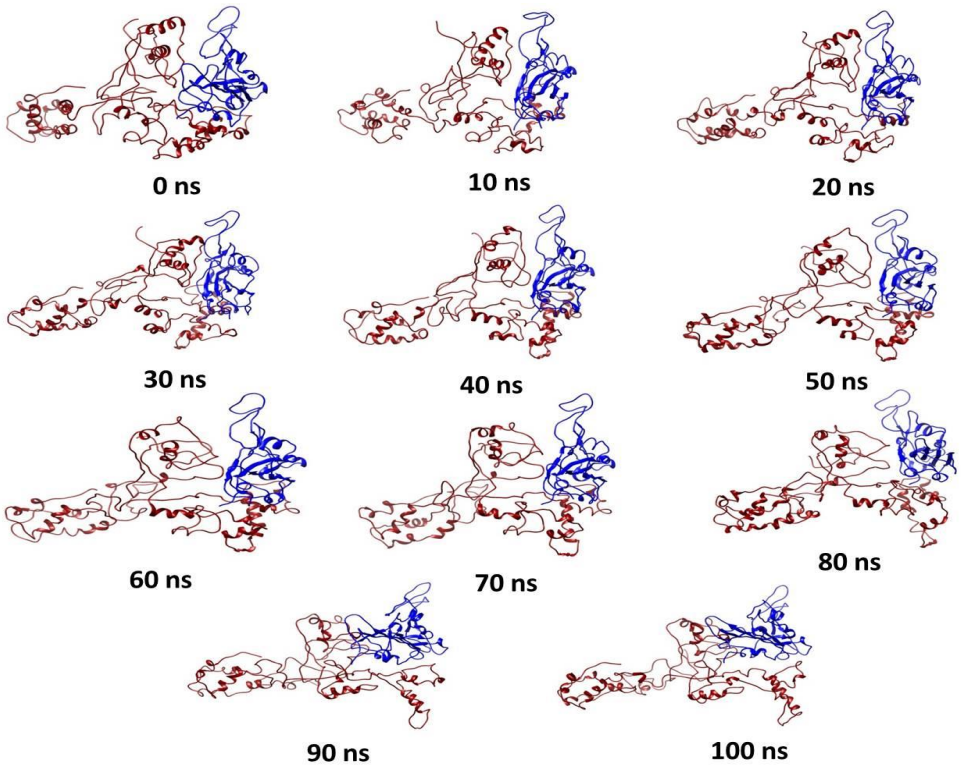

***Figure 12.2**. Conformational Snapshots of SARS-CoV-2 L-SIGN-Spike Protein structures at discrete interval of simulation time*

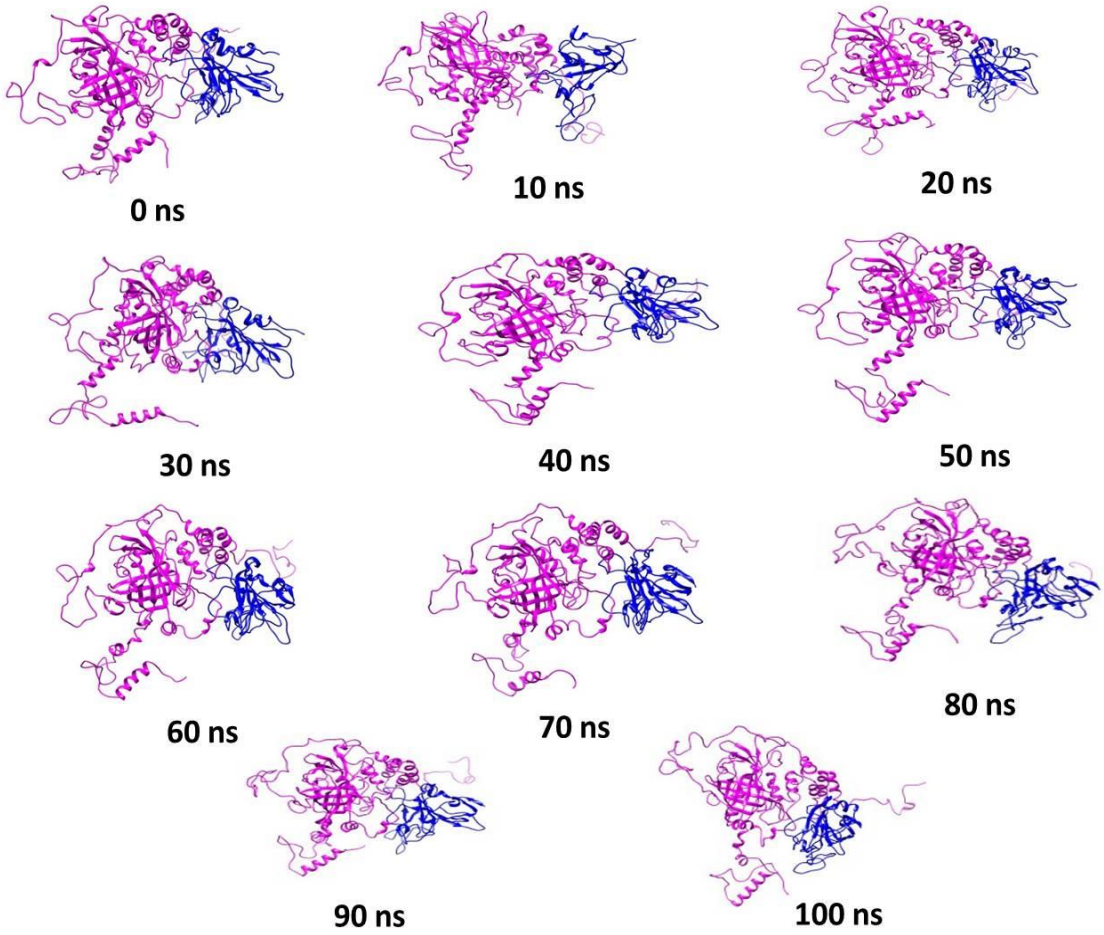

Figure 12.3. *Conformational Snapshots of SARS-CoV-2 CAT-Spike Protein structures at discrete interval of simulation time.*

12.3.6. Binding Free energy calculations.

HawkDock, a web server to predict the BFE and analyze the protein-protein complex based on computational docking and Generalized Born surface area continuum solvation (MM/GBSA) methods, was used to calculate the binding free energies of the (S protein-L-SIGN) and (S protein-CAT) complexes [48-50]. The overall binding free energies for the (S protein-L-SIGN) and (S protein-CAT) complexes were determined along with the other derived components (VDW, ELE, GB and SA) contributing to the overall BFE of the two complexes.

12.4.Results and Discussion:

12.4.1. MD Simulation analysis

To study the dynamic properties of the two complexes (SARS-CoV-2 Spike RBD bound with L-SIGN and CAT), we carried out 100 ns of MD simulation.

12.4.1.1.RMSD Analysis.

100 ns of MD simulation studies were carried out for both the complexes (S protein-L-SIGN) and (S protein-CAT) in order to get the dynamic properties of the two complexes. The RMSD (root mean square deviation) values of the back bone atoms of the complexes were obtained based on the average deviations in the atomic locations and the stability throughout the trajectory of 100 ns of the MD simulations is analyzed as depicted in **Figure 12.4.** The RMSD of L-SIGN as well as the CAT complex appeared to be stable after 10 ns, revealing that good convergence was achieved for each system. The average of RMSD is found to be approximately 2.09 Å (± 0.13) for the S protein-L-SIGN complex structure and 1.83 Å (± 0.16) for the S protein-CAT complex structure, inferring greater stability of the S protein-CAT complex as compared to the S protein-L-SIGN complex. Moreover, we also found the average of RMSD for the S protein-ACE2 complex structure to be 1.84 Å (± 0.12) according to our previous study [51]. Further, it was noticed that the stability of the S protein increases when bound to the receptors (CAT, L-SIGN and ACE2).

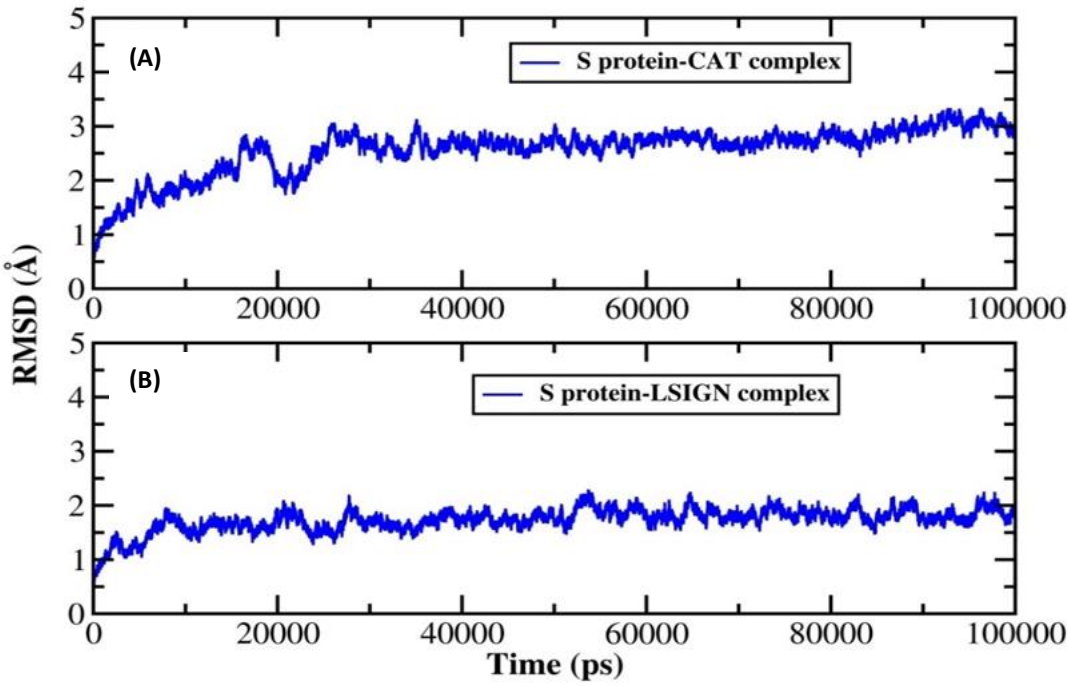

Figure 12.4. *The RMSD of the backbone Cα atoms for* ***(A)*** *S protein-L-SIGN complex and* ***(B)*** *S protein-CAT complex*

12.4.1.2.RMSF Analysis

We have analysed the root mean square fluctuations of backbone Cα atoms in the S protein-L-SIGN complex **(Figure 12.5)** and S protein-CAT complex **(Figure 12.6)**. We observed a significant difference in the flexibility of both complexes. When compared with the RMSF of the S protein-ACE2 complex

from our previous study [51], it was observed that the fluctuation in the S protein decreases when it is bound to the CAT and L-SIGN receptors. The S protein-L-SIGN and S protein-CAT complexes are therefore likely to be more stable than the S protein-ACE2 complex.

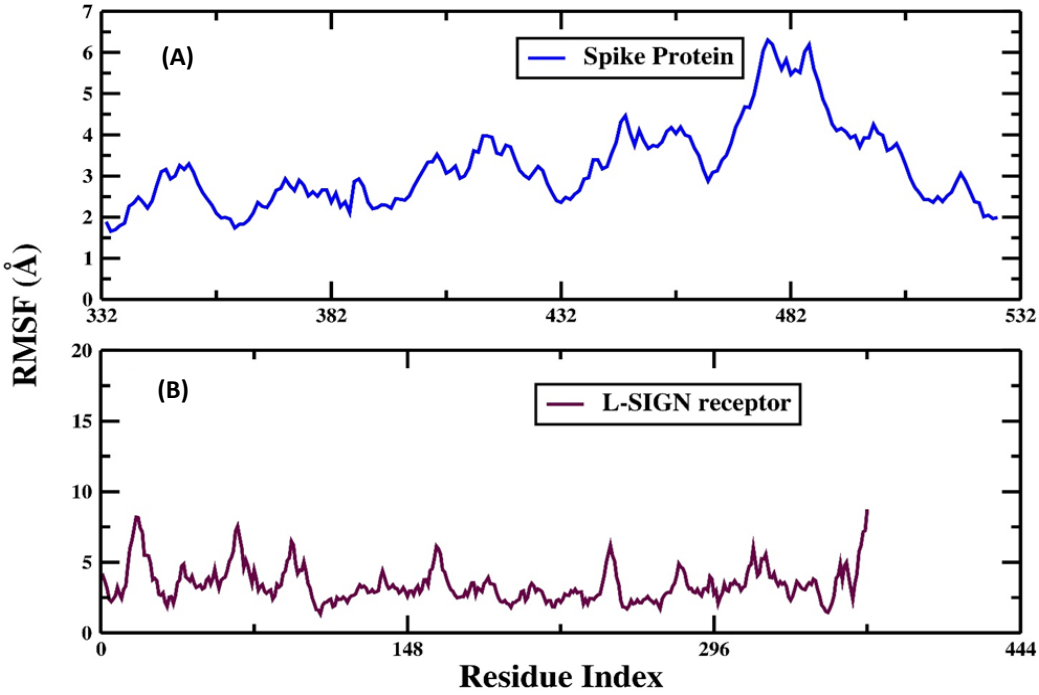

Figure 12.5. *The RMSF for the backbone Cα atoms* ***(A)*** *S protein* ***(B)*** *L-SIGN in S protein-L-SIGN complex.*

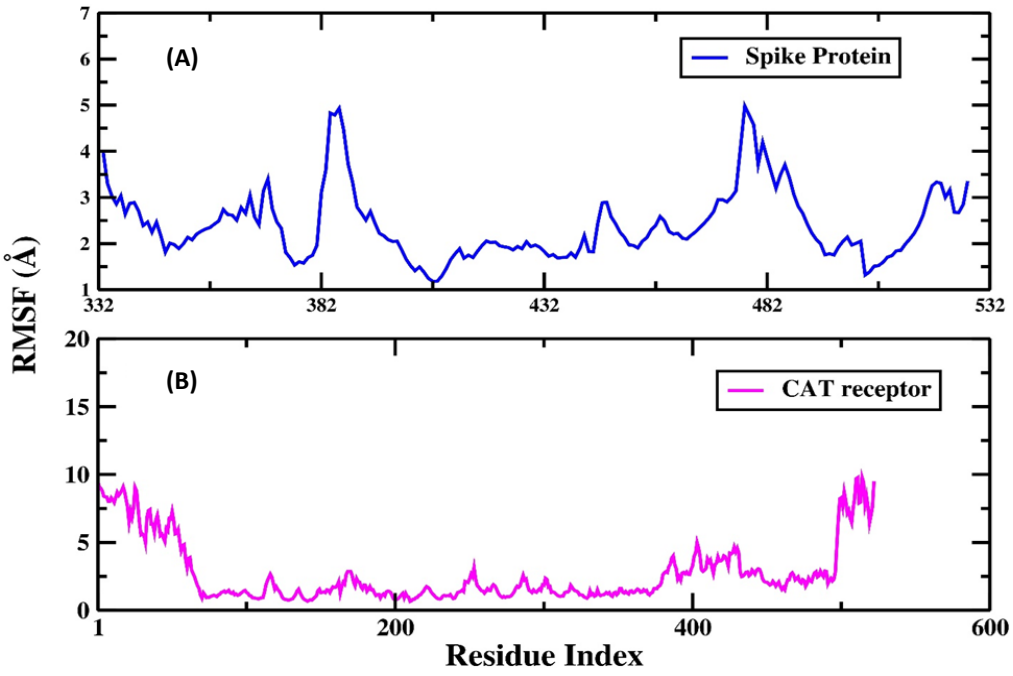

Figure 12.6. *The RMSF for the backbone Cα atoms* ***(A)*** *S protein* ***(B)*** *CAT in S protein-CAT complex*

12.4.1.3. Hydrogen bond Analysis

The hydrogen bonds play an important role in conferring stability to the protein complexes. So, here we calculated and plotted the number of intermolecular hydrogen bonds present in the (S protein-L-SIGN) and (S protein-CAT) complexes as depicted in **Figure 12.7.** The number of inter-molecular hy drogen bonds was found to be slightly higher in the S pro tein-CAT complex than in the S protein-L-SIGN complex hence inferring greater stability to the complex. Also, the number of inter-molecular hydrogen bonds for both com plexes was found to be relatively higher than the S protein ACE2 complex [51].

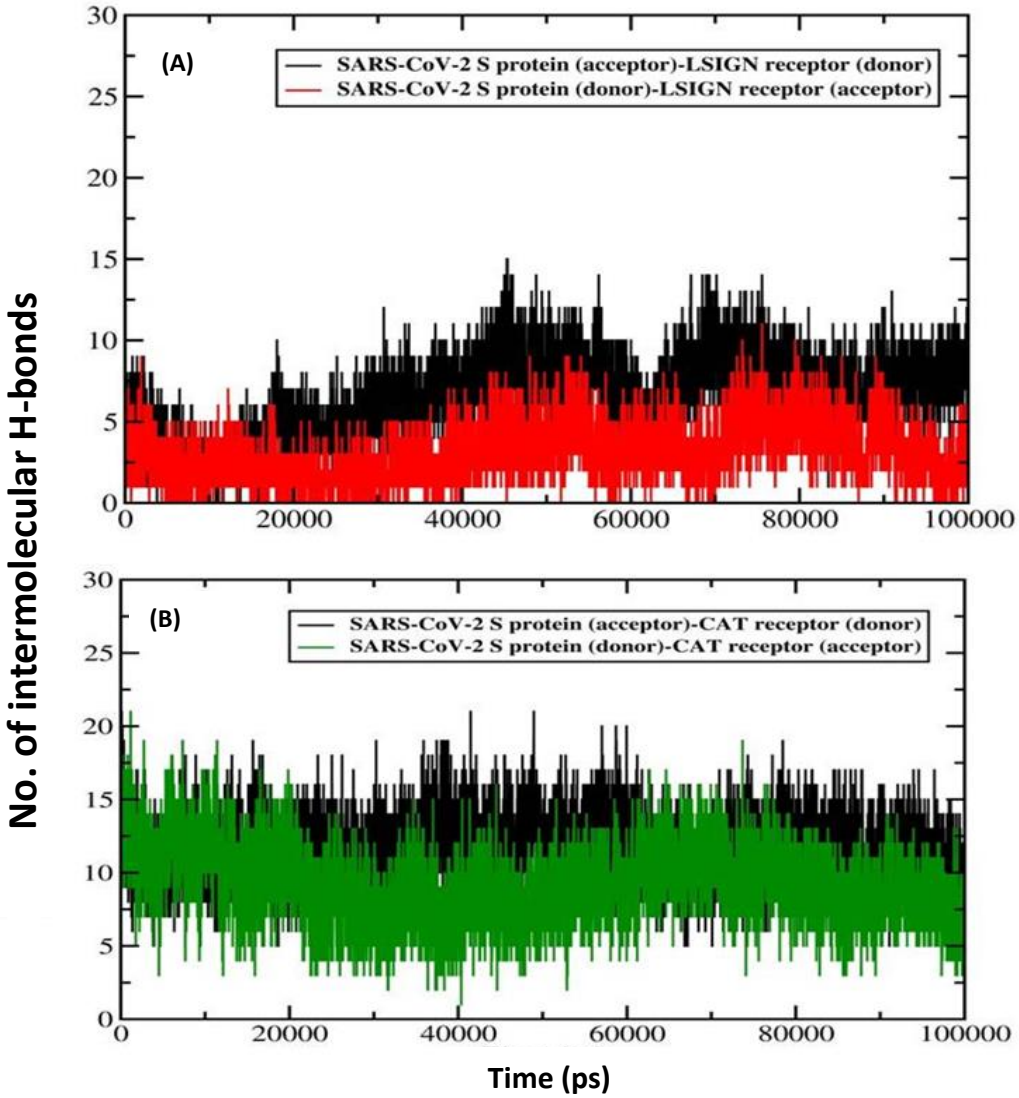

Figure 12.7. *The number of intermolecular hydrogen bonds between S protein and receptors in* ***(A)*** *S protein-L-SIGN complex* ***(B)*** *S protein-CAT complex obtained from 100ns of MD simulation*

In **Table 12.1-12.4,** we have listed out the intermolecular hydrogen bonds noticed between the S protein (acceptor/donor) and receptors (CAT, L-SIGN) (donor/acceptor) during the last 20 ns of MD simulation for both the complexes.

Table 12.1. *Hydrogen bond analysis of S protein-L-SIGN complex during the last 20 ns of MD simulation with S protein as acceptor and L-SIGN as donor.*

#Acceptor	DonorH	Donor	Frac	Average Distance (Å)	Average Angles (°)
ASN_108@O	ALA_334@H	ALA_334@N	0.2848	2.8614	154.9717
GLU_8@OE1	ARG_308@HH21	ARG_308@NH2	0.1338	2.8085	152.6348
GLU_8@OE1	ARG_308@HE	ARG_308@NE	0.1322	2.8337	156.2533
GLU_8@OE2	ARG_308@HH21	ARG_308@NH2	0.1237	2.8006	153.867
ASN_22@OD1	GLN_469@HE21	GLN_469@NE2	0.1182	2.8541	160.1179
ASN_2@OD1	LYS_388@HZ2	LYS_388@NZ	0.095	2.814	155.247
ASN_28@OD1	LYS_388@HZ3	LYS_388@NZ	0.092	2.8148	155.7004
ASN_28@OD1	LYS_388@HZ2	LYS_388@NZ	0.0853	2.8167	155.4032
GLU_8@OE2	ARG_308@HE	ARG_308@NE	0.0836	2.8348	155.9654
ASN_2@OD1	LYS_388@HZ1	LYS_388@NZ	0.0815	2.8058	155.5292
ARG_23@O	ARG_467@HE	ARG_467@NE	0.08	2.8295	151.1265
ASN_22@OD1	ARG_467@HH21	ARG_467@NH2	0.0784	2.842	153.0776
ASN_22@OD1	ARG_467@HE	ARG_467@NE	0.0774	2.8655	154.9174
ASN_2@OD1	LYS_388@HZ3	LYS_388@NZ	0.0733	2.8128	156.2279
SER_41@OG	LYS_319@HZ1	LYS_319@NZ	0.071	2.8584	153.968
SER_41@OG	LYS_319@HZ2	LYS_319@NZ	0.0708	2.8574	154.1554
ASN_28@OD1	LYS_388@HZ1	LYS_388@NZ	0.068	2.8222	155.5825
ASN_22@OD1	GLN_469@HE22	GLN_469@NE2	0.062	2.8552	161.4501
SER_41@OG	LYS_319@HZ3	LYS_319@NZ	0.0611	2.8541	153.5588
ARG_25@O	GLN_469@HE21	GLN_469@NE2	0.045	2.8768	161.9907
ARG_25@O	ARG_467@HH11	ARG_467@NH1	0.0406	2.828	153.0566
SER_27@O	LYS_390@HZ1	LYS_390@NZ	0.0358	2.8134	153.267
PRO_195@OXT	THR_376@HG1	THR_376@OG1	0.0352	2.7029	163.2477
SER_27@O	LYS_390@HZ3	LYS_390@NZ	0.0266	2.8213	153.8259
SER_27@O	LYS_390@HZ2	LYS_390@NZ	0.0256	2.8167	153.2492
ASN_28@O	LYS_388@HZ3	LYS_388@NZ	0.0256	2.8272	152.0951
ALA_20@O	GLN_469@HE21	GLN_469@NE2	0.0245	2.8729	161.9902
GLU_139@OE2	LYS_474@HZ1	LYS_474@NZ	0.0243	2.8081	159.2613
PRO_195@O	THR_376@HG1	THR_376@OG1	0.024	2.7039	165.2798
TRP_21@O	GLN_469@HE21	GLN_469@NE2	0.0237	2.8866	159.1855
GLU_139@OE2	LYS_474@HZ3	LYS_474@NZ	0.0204	2.8112	159.2395
ASN_28@O	LYS_390@HZ2	LYS_390@NZ	0.0204	2.8415	150.4481
ARG_23@O	ARG_467@HH21	ARG_467@NH2	0.0198	2.8194	145.968
ASN_2@OD1	LYS_390@HZ1	LYS_390@NZ	0.0174	2.8283	151.1424
ASN_28@O	LYS_390@HZ3	LYS_390@NZ	0.017	2.8367	150.6502
SER_39@O	LYS_319@HZ3	LYS_319@NZ	0.0169	2.82	148.3886

SER_39@O	LYS_319@HZ1	LYS_319@NZ	0.0163	2.8148	149.7552
SER_39@O	LYS_319@HZ2	LYS_319@NZ	0.0161	2.82	150.317
ASN_28@O	LYS_390@HZ1	LYS_390@NZ	0.0159	2.8453	149.6366
ASN_11@OD1	THR_307@HG1	THR_307@OG1	0.0156	2.7416	161.6031
ASN_2@OD1	LYS_390@HZ3	LYS_390@NZ	0.0155	2.8212	151.0807
ALA_40@O	LYS_319@HZ2	LYS_319@NZ	0.015	2.8329	156.3451
SER_27@OG	ARG_467@HH21	ARG_467@NH2	0.0138	2.855	155.5724
GLU_139@OE1	LYS_474@HZ1	LYS_474@NZ	0.0136	2.8077	156.6223
ASP_32@OD1	GLN_373@HE22	GLN_373@NE2	0.0134	2.8296	163.6244
ASN_2@OD1	LYS_390@HZ2	LYS_390@NZ	0.013	2.8267	150.9027
THR_1@O	GLN_392@HE22	GLN_392@NE2	0.0111	2.8658	157.111
ASN_28@O	LYS_388@HZ2	LYS_388@NZ	0.011	2.8348	148.557
ASN_28@O	LYS_388@HZ1	LYS_388@NZ	0.0099	2.8463	150.1378
SER_137@HB3	ILE_473@HA	ILE_473@CA	0.009	2.9307	146.2025
ARG_23@O	GLN_469@HE22	GLN_469@NE2	0.0082	2.8542	158.4547
GLU_139@OE2	LYS_474@HZ2	LYS_474@NZ	0.0078	2.8046	158.155
ARG_14@HG2	ASN_552@HA	ASN_552@CA	0.0075	2.9432	146.1692
ASN_2@OD1	LYS_390@H	LYS_390@N	0.0071	2.8806	156.8198
GLY_7@HA3	ALA_312@HA	ALA_312@CA	0.0064	2.9299	141.913
ALA_40@O	LYS_319@HZ3	LYS_319@NZ	0.0062	2.8284	150.4823
SER_41@HG	LYS_319@HZ3	LYS_319@NZ	0.006	2.8668	151.1486
ASN_28@HD21	LYS_388@HG2	LYS_388@CG	0.0057	2.8731	149.1621
ASN_108@HA	LEU_332@HA	LEU_332@CA	0.0057	2.9251	142.4389
ARG_23@O	GLN_469@HE21	GLN_469@NE2	0.0054	2.8469	152.9002
SER_41@HG	LYS_319@HZ1	LYS_319@NZ	0.005	2.8814	147.5267

Table 12.2. *Hydrogen bond analysis of S protein- L-SIGN complex during the last 20 ns of MD simulation with S protein as donor and L-SIGN as acceptor.*

#Acceptor	DonorH	Donor	Frac	Average Distance (Å)	Average Angles (°)
ASP_551@OD1	ARG_14@HH21	ARG_14@NH2	0.5133	2.8003	159.8873
THR_330@O	ASN_108@HD22	ASN_108@ND2	0.4934	2.8511	161.7927
ASP_551@OD2	ARG_14@HE	ARG_14@NE	0.4498	2.841	160.421
ASP_551@OD2	ARG_14@HH21	ARG_14@NH2	0.3548	2.8061	157.2295
ASP_551@OD2	ARG_14@H	ARG_14@N	0.3527	2.854	159.5868
ASP_551@OD2	THR_13@H	THR_13@N	0.263	2.858	154.3543
GLU_315@OE2	ASN_11@HD22	ASN_11@ND2	0.2415	2.8214	163.6516
ASP_551@OD1	ARG_14@HE	ARG_14@NE	0.2245	2.8462	160.8716
ASP_551@OD1	ARG_14@H	ARG_14@N	0.2143	2.8426	157.9829
ARG_331@O	ASN_107@HD22	ASN_107@ND2	0.182	2.8382	160.9025
ASP_551@OD1	THR_13@H	THR_13@N	0.1804	2.8538	156.7026
ALA_468@O	ARG_134@HH11	ARG_134@NH1	0.1742	2.8175	150.8829

GLU_387@O	ASN_28@HD21	ASN_28@ND2	0.1586	2.854	157.3339
VAL_466@O	ARG_25@HH11	ARG_25@NH1	0.1575	2.8117	157.4791
GLU_315@OE2	SER_41@HG	SER_41@OG	0.153	2.6699	162.6543
ALA_380@O	ASN_2@HD22	ASN_2@ND2	0.1452	2.8483	162.2086
GLN_469@OE1	ARG_25@H	ARG_25@N	0.1312	2.8586	161.8669
GLU_465@OE1	SER_27@HG	SER_27@OG	0.1289	2.6691	163.6608
GLN_469@OE1	ARG_23@H	ARG_23@N	0.114	2.8736	160.2489
GLU_315@OE1	SER_41@HG	SER_41@OG	0.1006	2.6836	163.3554
GLU_377@OE1	LYS_54@HZ2	LYS_54@NZ	0.0972	2.7854	159.9101
GLU_377@OE2	LYS_54@HZ3	LYS_54@NZ	0.0789	2.7782	159.6595
GLU_377@O	THR_1@HG1	THR_1@OG1	0.0744	2.7271	163.33
ALA_381@O	ASN_2@H	ASN_2@N	0.0738	2.8679	161.1065
LYS_390@O	THR_1@H2	THR_1@N	0.0728	2.8182	152.3783
LYS_390@O	THR_1@H1	THR_1@N	0.0687	2.8196	152.2007
GLN_464@O	ARG_25@HH11	ARG_25@NH1	0.0596	2.8477	156.673
GLU_377@OE1	LYS_54@HZ1	LYS_54@NZ	0.0545	2.7812	158.0505
LYS_390@O	THR_1@H3	THR_1@N	0.0539	2.8195	151.2948
GLU_465@OE2	SER_27@HG	SER_27@OG	0.0536	2.6935	162.121
GLU_377@OE2	LYS_54@HZ2	LYS_54@NZ	0.0516	2.7939	156.0613
ALA_312@O	ASN_11@HD21	ASN_11@ND2	0.0494	2.8467	158.4731
ASP_549@OD1	LYS_24@HZ3	LYS_24@NZ	0.0491	2.8186	154.7262
GLU_377@OE2	LYS_54@HZ1	LYS_54@NZ	0.0435	2.7819	157.049
ASP_551@OD1	THR_13@HG1	THR_13@OG1	0.0422	2.7106	161.0699
ASP_549@OD2	LYS_24@HZ1	LYS_24@NZ	0.042	2.8214	154.0752
LYS_333@O	ASN_108@HD22	ASN_108@ND2	0.038	2.8701	154.7872
ASP_549@OD1	LYS_24@HZ1	LYS_24@NZ	0.036	2.8207	155.1742
ASP_549@OD2	LYS_24@HZ3	LYS_24@NZ	0.0356	2.8274	152.5154
GLU_387@OE1	ASN_28@HD21	ASN_28@ND2	0.0353	2.8429	160.2944
ASP_549@OD2	LYS_24@HZ2	LYS_24@NZ	0.0347	2.8261	154.0473
GLU_387@OE2	ASN_28@HD21	ASN_28@ND2	0.0306	2.841	159.47
GLU_374@OE2	LYS_54@HZ1	LYS_54@NZ	0.0302	2.79	157.2421
GLU_374@OE1	LYS_54@HZ1	LYS_54@NZ	0.0291	2.7835	156.5435
ASP_551@OD2	THR_13@HG1	THR_13@OG1	0.028	2.7184	159.6033
ASP_549@O	LYS_24@HZ1	LYS_24@NZ	0.0263	2.8342	153.112
GLU_374@OE1	LYS_54@HZ3	LYS_54@NZ	0.0257	2.7808	157.1073
ASP_549@OD1	LYS_24@HZ2	LYS_24@NZ	0.0254	2.8245	154.3738
GLU_374@OE2	LYS_54@HZ2	LYS_54@NZ	0.022	2.7738	157.7041
GLU_374@OE2	LYS_54@HZ3	LYS_54@NZ	0.0214	2.7835	157.3532
GLU_364@OE1	THR_1@H3	THR_1@N	0.0204	2.8073	155.9293
GLU_364@OE1	THR_1@H1	THR_1@N	0.019	2.813	154.2079
LEU_378@O	THR_1@HG1	THR_1@OG1	0.0178	2.773	161.9267
GLU_374@OE1	LYS_54@HZ2	LYS_54@NZ	0.0175	2.7843	156.3019
ASP_549@O	LYS_24@HZ2	LYS_24@NZ	0.0165	2.8339	151.2607
ASP_549@O	LYS_24@HZ3	LYS_24@NZ	0.0163	2.832	151.4358

GLU_315@OE2	ASN_11@HD21	ASN_11@ND2	0.0161	2.8017	163.1959
THR_307@O	ASN_11@HD21	ASN_11@ND2	0.0158	2.8727	157.9253
GLN_392@OE1	THR_1@H1	THR_1@N	0.0158	2.827	149.8726
GLN_392@OE1	THR_1@H3	THR_1@N	0.0158	2.8226	149.8199
GLN_392@OE1	THR_1@H2	THR_1@N	0.0151	2.8312	149.8318
LYS_388@O	ASN_2@HD21	ASN_2@ND2	0.0141	2.8537	153.3506
THR_376@OG1	THR_1@HG1	THR_1@OG1	0.0132	2.813	159.9506
GLU_377@OE1	LYS_54@HZ3	LYS_54@NZ	0.0128	2.7961	155.1329
GLU_364@OE1	THR_1@H2	THR_1@N	0.0114	2.806	157.014
ARG_308@O	ASN_11@HD22	ASN_11@ND2	0.0113	2.8662	150.3261
ASN_552@HA	ARG_14@HG2	ARG_14@CG	0.0106	2.9427	144.2634
LEU_332@O	ASN_107@HD22	ASN_107@ND2	0.01	2.8469	158.5659
THR_330@OG1	ASN_108@HD22	ASN_108@ND2	0.01	2.9006	164.7733
GLU_315@OE2	SER_39@HG	SER_39@OG	0.0096	2.7025	162.5934
ARG_308@O	ASN_11@HD21	ASN_11@ND2	0.0095	2.863	153.3976
GLN_469@HB2	ARG_23@H	ARG_23@N	0.0091	2.8843	151.0592
GLU_364@OE1	THR_1@HG1	THR_1@OG1	0.0085	2.6952	161.035
LEU_391@O	THR_1@H2	THR_1@N	0.0077	2.8585	145.8976
ILE_473@HA	SER_137@HB3	SER_137@CB	0.0077	2.9308	147.907
LYS_388@O	ASN_2@HD22	ASN_2@ND2	0.0076	2.8473	152.4258
GLU_364@OE2	THR_1@H3	THR_1@N	0.0076	2.8109	149.8045
LEU_391@O	THR_1@H3	THR_1@N	0.0072	2.8585	144.5775
GLU_315@OE1	SER_39@HG	SER_39@OG	0.0072	2.7122	163.427
GLN_469@HE21	ASN_22@HA	ASN_22@CA	0.0069	2.8969	143.4412
VAL_550@O	ASN_22@HD21	ASN_22@ND2	0.0067	2.9047	156.9303
GLU_364@OE2	THR_1@H1	THR_1@N	0.0065	2.7952	151.6534
LYS_388@O	THR_1@H1	THR_1@N	0.0064	2.7993	144.1739
ASP_551@OD2	ARG_14@HH12	ARG_14@NH1	0.0064	2.7988	157.4174
ALA_311@O	GLY_7@H	GLY_7@N	0.006	2.8608	155.8292
ARG_331@O	ASN_108@HD22	ASN_108@ND2	0.006	2.8744	160.9081
GLU_364@OE2	THR_1@H2	THR_1@N	0.006	2.7891	152.0915
LEU_391@O	THR_1@H1	THR_1@N	0.0058	2.8702	145.8486
THR_376@OG1	LYS_54@HZ1	LYS_54@NZ	0.0058	2.8614	158.5293
GLN_464@OE1	ARG_25@HH12	ARG_25@NH1	0.0056	2.8171	152.679
LEU_332@O	ASN_107@HD21	ASN_107@ND2	0.0054	2.8388	146.6063
THR_376@OG1	LYS_54@HZ3	LYS_54@NZ	0.0054	2.8474	157.9546
LEU_385@HD11	ASN_2@H	ASN_2@N	0.0052	2.8089	149.9837
LYS_388@O	THR_1@H3	THR_1@N	0.0051	2.8321	145.3553

Table 12.3. *Hydrogen bond analysis of S protein-CAT complex during the last 20 ns of MD simulation with S protein as acceptor and CAT as donor.*

#Acceptor	DonorH	Donor	Frac	Average Distance (Å)	Average Angles (°)
VAL_75@O	SER_441@H	SER_441@N	0.7047	2.8555	160.1122
ASP_73@OD1	ARG_322@HH22	ARG_322@NH2	0.7035	2.7892	161.6997
ASP_73@OD2	ARG_322@HH11	ARG_322@NH1	0.6994	2.8093	163.5115
PRO_167@O	GLN_670@HE21	GLN_670@NE2	0.5853	2.845	162.4634
ARG_76@O	SER_449@HG	SER_449@OG	0.554	2.7448	161.7508
GLN_174@OE1	ALA_659@H	ALA_659@N	0.5418	2.8713	160.5658
GLU_74@O	ASP_444@H	ASP_444@N	0.5283	2.8407	151.0588
GLU_74@O	GLU_443@H	GLU_443@N	0.4858	2.8759	152.9664
GLY_115@O	ASN_696@H	ASN_696@N	0.3154	2.8602	159.6656
GLN_174@OE1	ILE_658@H	ILE_658@N	0.2989	2.8604	150.8622
GLN_77@O	ALA_446@H	ALA_446@N	0.2406	2.893	160.2217
ASN_169@OD1	LEU_662@H	LEU_662@N	0.1466	2.9156	160.1472
ASP_95@OD2	ARG_447@HH11	ARG_447@NH1	0.1412	2.792	154.7283
ASP_73@OD2	ARG_322@HH22	ARG_322@NH2	0.1384	2.8125	156.3612
THR_168@OG1	GLY_660@H	GLY_660@N	0.1254	2.9125	156.8478
GLN_82@OE1	GLN_450@HE21	GLN_450@NE2	0.1132	2.8517	161.5789
GLN_166@OE1	GLN_670@HE22	GLN_670@NE2	0.106	2.8639	162.5295
GLN_77@O	ARG_447@H	ARG_447@N	0.1001	2.8466	146.8759
ASP_95@OD1	ARG_447@HH11	ARG_447@NH1	0.0941	2.8013	154.1576
VAL_171@O	ARG_322@HH12	ARG_322@NH1	0.0936	2.811	152.712
ASP_95@OD2	ARG_447@HH22	ARG_447@NH2	0.0855	2.824	150.3213
GLN_77@O	GLN_450@HE21	GLN_450@NE2	0.0766	2.8289	157.8841
ASP_95@OD1	ARG_447@HH22	ARG_447@NH2	0.0751	2.8222	151.4778
ASN_116@OD1	ASN_696@HD22	ASN_696@ND2	0.0708	2.8708	161.5225
THR_83@O	GLN_450@HE22	GLN_450@NE2	0.0646	2.8708	159.1468
GLN_77@OE1	SER_449@HG	SER_449@OG	0.0532	2.724	159.9681
ASN_149@O	HIE_713@HE2	HIE_713@NE2	0.0523	2.8452	157.6379
ARG_76@HD2	VAL_442@HA	VAL_442@CA	0.0493	2.9343	148.3705
GLN_166@O	GLY_660@H	GLY_660@N	0.049	2.8668	161.5909
ASN_116@OD1	ASN_696@HD21	ASN_696@ND2	0.0458	2.847	161.0551
GLN_77@O	GLN_450@HE22	GLN_450@NE2	0.0444	2.8343	153.5234
ILE_78@O	ALA_445@H	ALA_445@N	0.0428	2.8357	145.1541
VAL_113@O	LYS_694@HZ1	LYS_694@NZ	0.0418	2.8156	149.4991
VAL_113@O	LYS_694@HZ3	LYS_694@NZ	0.0394	2.8147	151.7217
SER_111@O	LYS_694@HZ3	LYS_694@NZ	0.0382	2.8303	151.9852
VAL_113@O	LYS_694@HZ2	LYS_694@NZ	0.0372	2.8192	150.017
SER_111@O	LYS_694@HZ1	LYS_694@NZ	0.0358	2.8379	152.3057
SER_111@O	LYS_694@HZ2	LYS_694@NZ	0.0308	2.8368	152.2202
GLU_74@H	SER_441@HB3	SER_441@CB	0.03	2.8833	145.5468

THR_168@H	ALA_659@HA	ALA_659@CA	0.0286	2.9008	153.4567
GLN_174@HE21	GLU_656@HA	GLU_656@CA	0.0272	2.9085	146.3871
GLN_161@OE1	LYS_663@HZ2	LYS_663@NZ	0.0263	2.8187	153.5414
ASP_110@O	LYS_694@HZ1	LYS_694@NZ	0.0261	2.8261	152.1725
ASN_169@OD1	HIE_661@H	HIE_661@N	0.0246	2.8644	151.2584
ASN_116@O	LYS_694@HZ2	LYS_694@NZ	0.0246	2.8298	157.997
GLY_115@O	LYS_694@HZ2	LYS_694@NZ	0.0232	2.8179	154.3661
ASN_169@HD21	HIE_661@H	HIE_661@N	0.0224	2.8979	146.213
GLN_82@OE1	GLN_450@HE22	GLN_450@NE2	0.0217	2.8732	157.7109
GLN_161@OE1	LYS_663@HZ3	LYS_663@NZ	0.0216	2.8232	152.2353
THR_83@OG1	GLN_450@HE22	GLN_450@NE2	0.0211	2.8696	154.4757
GLU_74@H	SER_441@HB2	SER_441@CB	0.0208	2.8321	146.6557
GLN_161@OE1	LYS_663@HZ1	LYS_663@NZ	0.0199	2.8161	153.4922
TYR_163@O	TYR_695@HH	TYR_695@OH	0.0198	2.7752	156.1283
ASP_110@O	LYS_694@HZ2	LYS_694@NZ	0.0192	2.8242	151.0537
ASP_110@O	LYS_694@HZ3	LYS_694@NZ	0.0185	2.8185	152.5714
GLY_115@O	LYS_694@HZ3	LYS_694@NZ	0.0173	2.8178	154.4665
TYR_173@HB3	GLY_660@HA2	GLY_660@CA	0.0171	2.9391	142.9172
ASN_116@O	LYS_694@HZ1	LYS_694@NZ	0.0168	2.828	157.2326
GLY_172@O	ARG_322@HH11	ARG_322@NH1	0.0166	2.8205	146.4888
GLN_166@OE1	TYR_695@HH	TYR_695@OH	0.0161	2.7512	159.7219
GLU_74@HB3	SER_441@HB2	SER_441@CB	0.0152	2.9202	140.9111
PRO_80@O	ARG_447@HH22	ARG_447@NH2	0.0149	2.8414	149.6966
ASN_116@O	LYS_694@HZ3	LYS_694@NZ	0.0144	2.8275	158.6773
TYR_173@HB2	GLY_660@HA2	GLY_660@CA	0.0144	2.9413	141.6586
GLY_114@O	ASN_696@HD22	ASN_696@ND2	0.0138	2.8462	156.6316
GLY_115@O	LYS_694@HZ1	LYS_694@NZ	0.0136	2.8196	152.5946
SER_43@O	ARG_653@HH21	ARG_653@NH2	0.0124	2.8519	151.3182
SER_43@OG	LYS_652@HZ1	LYS_652@NZ	0.0116	2.8702	149.7739
PRO_167@HD3	LEU_691@HB3	LEU_691@CB	0.0113	2.9349	142.9347
ALA_40@O	LYS_652@HZ3	LYS_652@NZ	0.011	2.8153	151.0345
ASN_169@H	GLY_660@HA3	GLY_660@CA	0.011	2.8581	149.7505
SER_162@OG	LYS_663@HZ1	LYS_663@NZ	0.0108	2.8577	151.7519
GLN_82@HE21	ARG_447@HA	ARG_447@CA	0.0106	2.877	143.516
GLY_114@O	GLU_698@H	GLU_698@N	0.0104	2.8776	154.6572
GLN_77@HA	SER_449@HB2	SER_449@CB	0.0102	2.9301	140.9467
GLN_82@OE1	ARG_447@HE	ARG_447@NE	0.0098	2.8295	156.0532
GLY_172@HA2	ASN_657@HA	ASN_657@CA	0.0096	2.9423	144.9956
SER_43@OG	LYS_652@HZ3	LYS_652@NZ	0.0094	2.8696	149.6534
GLN_82@OE1	ARG_447@HH12	ARG_447@NH1	0.0092	2.8246	156.3896
THR_168@HG1	GLY_660@H	GLY_660@N	0.0092	2.9334	148.2941
GLY_170@H	GLY_660@HA3	GLY_660@CA	0.009	2.8524	142.1464
SER_43@OG	LYS_652@HZ2	LYS_652@NZ	0.0087	2.8633	150.6857
GLU_74@HB2	SER_441@HB2	SER_441@CB	0.0087	2.9254	140.2436

TYR_163@O	LYS_699@HZ2	LYS_699@NZ	0.0086	2.8344	160.2672
GLY_115@O	ALA_697@H	ALA_697@N	0.0086	2.9151	160.5222
PRO_167@HA	ALA_659@HA	ALA_659@CA	0.0086	2.9275	144.3862
GLN_166@HE22	LYS_694@HB2	LYS_694@CB	0.0079	2.9103	143.8331
SER_162@OG	LYS_663@HZ3	LYS_663@NZ	0.0078	2.8646	150.2729
PRO_167@HD3	LEU_691@HG	LEU_691@CG	0.0076	2.9406	143.7664
ASN_116@HA	ASN_696@H	ASN_696@N	0.0076	2.8884	144.4572
ALA_40@O	LYS_652@HZ1	LYS_652@NZ	0.0075	2.8212	147.5299
TYR_176@HH	GLU_656@HB3	GLU_656@CB	0.0073	2.892	142.9173
ARG_76@HB2	VAL_442@HA	VAL_442@CA	0.0072	2.9135	139.1321
ILE_78@HG21	ASP_444@HA	ASP_444@CA	0.0071	2.9436	143.3538
SER_162@OG	LYS_663@HZ2	LYS_663@NZ	0.007	2.8649	149.2892
GLY_72@O	SER_396@HG	SER_396@OG	0.0069	2.8116	155.8801
ARG_71@HE	ARG_322@HH22	ARG_322@NH2	0.0069	2.8941	140.6713
SER_43@O	ARG_653@HH22	ARG_653@NH2	0.0066	2.8307	150.1017
GLN_166@OE1	ALA_665@H	ALA_665@N	0.0066	2.9022	154.4796
GLN_174@HE21	ILE_658@HG22	ILE_658@CG2	0.0066	2.8718	145.5068
GLN_174@HE21	ILE_658@HG23	ILE_658@CG2	0.0065	2.8924	144.3953
PRO_80@O	ARG_447@HH11	ARG_447@NH1	0.0065	2.8354	152.0107
ASP_95@OD1	ARG_447@HH12	ARG_447@NH1	0.0064	2.8249	158.9373
GLY_115@HA2	LYS_694@HA	LYS_694@CA	0.0062	2.9325	140.9355
ASN_118@OD1	LYS_694@HZ3	LYS_694@NZ	0.006	2.8266	150.8576
GLN_77@HE22	GLN_450@HB2	GLN_450@CB	0.0059	2.8839	146.0987
ILE_78@HG23	ASP_444@HA	ASP_444@CA	0.0059	2.9446	142.8395
ASN_105@OD1	LYS_652@HZ3	LYS_652@NZ	0.0058	2.8253	151.474
GLU_74@OE1	SER_396@HG	SER_396@OG	0.0058	2.658	160.023
ARG_76@HA	LEU_440@HD23	LEU_440@CD2	0.0058	2.9439	145.2484
GLU_74@OE2	ARG_653@HE	ARG_653@NE	0.0056	2.8708	153.7432
GLN_174@HE22	HIE_687@HE2	HIE_687@NE2	0.0056	2.9051	146.8238
PRO_80@O	ARG_447@HH12	ARG_447@NH1	0.0055	2.8268	146.2336
ASP_73@OD1	ARG_322@HH11	ARG_322@NH1	0.0053	2.9128	144.0935
ILE_78@HG22	ASP_444@HA	ASP_444@CA	0.0053	2.9416	143.6256
SER_162@O	LYS_663@HZ3	LYS_663@NZ	0.0052	2.8386	152.0758
ALA_79@HB3	ALA_446@H	ALA_446@N	0.0052	2.8686	146.9945
ALA_79@HB1	ALA_446@H	ALA_446@N	0.005	2.8826	148.63

Table 12.4. *Hydrogen bond analysis of S protein-CAT complex during the last 20 ns of MD simulation with S protein as donor and CAT as acceptor.*

#Acceptor	DonorH	Donor	Frac	Average Distance (Å)	Average Angles (º)
ASP_444@O	ARG_76@H	ARG_76@N	0.9486	2.8111	164.6075
LEU_662@O	THR_168@HG1	THR_168@OG1	0.7456	2.7476	162.9437
GLU_656@OE2	ASN_107@HD22	ASN_107@ND2	0.6328	2.8281	164.8966

GLU_443@OE1	ARG_71@HH22	ARG_71@NH2	0.5279	2.7773	158.4681
GLU_443@O	GLN_77@H	GLN_77@N	0.4509	2.8784	151.9572
ASN_657@O	VAL_171@H	VAL_171@N	0.4257	2.8769	160.8309
ASN_657@OD1	GLY_172@H	GLY_172@N	0.3812	2.8824	159.2124
GLU_443@O	ILE_78@H	ILE_78@N	0.3805	2.8534	153.869
GLU_656@OE1	ASN_105@HD22	ASN_105@ND2	0.3597	2.8459	161.8646
ASP_319@OD2	ARG_76@HH12	ARG_76@NH1	0.3402	2.7967	153.1788
ASP_319@OD1	ARG_76@HH11	ARG_76@NH1	0.2814	2.7991	159.2412
ASP_319@OD2	ARG_76@HH22	ARG_76@NH2	0.2684	2.8098	149.8818
GLU_443@OE2	ARG_71@HH22	ARG_71@NH2	0.237	2.7766	159.3117
ASP_693@O	GLN_166@HE22	GLN_166@NE2	0.2046	2.85	161.552
GLU_656@OE2	GLN_174@HE22	GLN_174@NE2	0.1957	2.7977	150.4254
ASP_444@OD2	LYS_46@HZ1	LYS_46@NZ	0.1766	2.7718	156.6219
GLU_656@OE1	ASN_105@HD21	ASN_105@ND2	0.1554	2.8384	163.2509
ASP_444@OD2	LYS_46@HZ2	LYS_46@NZ	0.1496	2.7715	157.1805
HIE_661@ND1	ASN_169@HD21	ASN_169@ND2	0.1416	2.917	152.9534
ASP_444@OD2	LYS_46@HZ3	LYS_46@NZ	0.1344	2.7708	156.9466
ILE_658@O	THR_168@H	THR_168@N	0.1256	2.9028	157.8484
ASP_693@OD2	GLY_115@H	GLY_115@N	0.1202	2.8683	158.4398
GLN_450@OE1	GLN_77@HE22	GLN_77@NE2	0.1191	2.8366	158.18
ASP_444@OD1	LYS_46@HZ1	LYS_46@NZ	0.1185	2.7723	156.8832
SER_441@O	GLU_74@H	GLU_74@N	0.0957	2.9153	159.6169
ASP_444@OD1	LYS_46@HZ3	LYS_46@NZ	0.0914	2.773	158.7997
GLU_443@OE1	ARG_71@HH12	ARG_71@NH1	0.0892	2.8479	148.3398
HIE_687@ND1	ASN_108@HD22	ASN_108@ND2	0.0812	2.9122	160.093
GLN_450@OE1	GLN_82@HE22	GLN_82@NE2	0.0724	2.8423	159.8648
ASP_444@O	GLN_77@H	GLN_77@N	0.0688	2.802	141.8012
ASP_319@OD2	ARG_76@HH11	ARG_76@NH1	0.0648	2.7982	156.7966
ASP_444@OD1	LYS_46@HZ2	LYS_46@NZ	0.0636	2.7799	156.3437
ARG_447@O	GLN_82@HE21	GLN_82@NE2	0.0573	2.8827	156.3259
LYS_694@O	GLN_166@HE22	GLN_166@NE2	0.0561	2.8528	151.7299
ALA_659@HA	THR_168@H	THR_168@N	0.0518	2.8779	149.9434
GLN_450@OE1	THR_83@HG1	THR_83@OG1	0.0515	2.7683	160.5969
TYR_695@OH	SER_162@HG	SER_162@OG	0.0513	2.8218	160.037
VAL_442@HA	ARG_76@HD2	ARG_76@CD	0.051	2.9208	142.8311
GLN_450@OE1	THR_83@H	THR_83@N	0.0472	2.8485	160.4471
ASP_693@OD1	GLY_115@H	GLY_115@N	0.0459	2.8846	158.5326
CYS_655@O	GLN_174@HE21	GLN_174@NE2	0.0424	2.8983	154.3182
GLU_649@OE1	SER_43@HG	SER_43@OG	0.04	2.7099	163.1139
ASN_657@O	GLY_172@H	GLY_172@N	0.0389	2.8959	154.2287
HIE_687@O	ASN_108@HD21	ASN_108@ND2	0.0363	2.8636	152.6256
SER_441@HB3	GLU_74@H	GLU_74@N	0.0362	2.8584	143.7025
SER_449@O	GLN_77@HE22	GLN_77@NE2	0.0357	2.8697	159.5434
GLU_656@OE1	ASN_107@HD22	ASN_107@ND2	0.0305	2.8415	164.3923

GLU_649@OE2	SER_43@HG	SER_43@OG	0.0287	2.6952	164.0282
GLN_450@OE1	GLN_82@HE21	GLN_82@NE2	0.0287	2.842	159.9156
GLU_656@OE2	ASN_105@HD22	ASN_105@ND2	0.0284	2.8511	160.4425
HIE_661@H	ASN_169@HD21	ASN_169@ND2	0.0276	2.8945	144.6222
SER_449@OG	ARG_76@HH21	ARG_76@NH2	0.0264	2.879	156.9624
SER_686@O	ASN_108@HD21	ASN_108@ND2	0.0264	2.859	150.5495
ASP_319@OD1	ARG_76@HE	ARG_76@NE	0.025	2.8722	149.8167
LYS_663@O	GLN_166@HE22	GLN_166@NE2	0.0228	2.8465	156.343
ASP_444@HB3	GLU_74@HA	GLU_74@CA	0.0226	2.933	140.9535
LYS_663@O	GLN_166@HE21	GLN_166@NE2	0.0216	2.8587	152.3819
GLU_698@OE2	ASN_116@HD22	ASN_116@ND2	0.0214	2.8206	161.7276
PHE_395@HE2	VAL_171@H	VAL_171@N	0.0203	2.8088	146.2483
GLU_656@OE2	ASN_105@HD21	ASN_105@ND2	0.0202	2.8515	156.9697
SER_441@HB2	GLU_74@HB3	GLU_74@CB	0.0192	2.9165	140.4043
GLU_698@OE1	ASN_116@HD22	ASN_116@ND2	0.0189	2.8218	162.5682
SER_449@O	GLN_77@HE21	GLN_77@NE2	0.0169	2.883	159.6835
GLY_660@HA3	ASN_169@H	ASN_169@N	0.0165	2.84	151.4003
LYS_372@O	ASN_169@HD22	ASN_169@ND2	0.016	2.8654	160.0378
ALA_690@O	LYS_112@HZ3	LYS_112@NZ	0.0156	2.8182	154.2844
LEU_691@HB3	PRO_167@HD3	PRO_167@CD	0.0154	2.9432	145.9466
ALA_690@O	SER_111@HG	SER_111@OG	0.0147	2.7396	160.6911
ASP_319@OD2	ARG_76@HE	ARG_76@NE	0.0143	2.8541	151.0787
ARG_447@HA	GLN_82@HE21	GLN_82@NE2	0.0136	2.8175	143.7613
HIE_713@O	ASN_149@HD21	ASN_149@ND2	0.0134	2.8577	158.74
VAL_442@HA	ARG_76@HB2	ARG_76@CB	0.0133	2.9318	140.514
GLU_443@OE2	ARG_71@HH12	ARG_71@NH1	0.0131	2.857	147.5152
ILE_658@HG23	GLN_174@HE21	GLN_174@NE2	0.013	2.8353	143.1683
GLN_450@OE1	GLN_77@HE21	GLN_77@NE2	0.012	2.8561	154.69
ILE_658@HG22	GLN_174@HE21	GLN_174@NE2	0.0118	2.8359	143.9562
ILE_658@O	GLY_170@H	GLY_170@N	0.0118	2.9043	145.4256
SER_449@HG	GLN_77@HA	GLN_77@CA	0.0115	2.9165	142.1307
ASP_693@OD2	LYS_112@HZ2	LYS_112@NZ	0.0114	2.8069	158.9852
ILE_658@HG12	GLN_174@HE21	GLN_174@NE2	0.0109	2.8681	143.7305
ALA_659@HA	PRO_167@HA	PRO_167@CA	0.0108	2.931	144.078
ALA_659@O	TYR_173@H	TYR_173@N	0.0107	2.8773	149.4746
GLY_660@HA2	TYR_173@HB3	TYR_173@CB	0.0102	2.9298	142.4943
ARG_322@HH22	ARG_71@HE	ARG_71@NE	0.0102	2.9001	142.5842
LEU_691@HG	PRO_167@HD3	PRO_167@CD	0.0093	2.9391	144.9276
SER_449@HB2	GLN_77@HA	GLN_77@CA	0.009	2.9364	144.8425
LYS_694@HA	GLY_115@HA2	GLY_115@CA	0.009	2.9407	142.056
GLY_660@HA3	GLY_170@H	GLY_170@N	0.0089	2.7849	142.2742
ALA_445@HB2	ALA_79@HA	ALA_79@CA	0.0084	2.9494	145.5964
ASN_657@HA	GLY_172@HA2	GLY_172@CA	0.0084	2.9308	143.4228
ASN_696@O	TYR_117@H	TYR_117@N	0.0082	2.9065	152.9378

ALA_690@HA	LYS_112@HA	LYS_112@CA	0.008	2.9379	147.3597
GLY_660@H	GLY_170@H	GLY_170@N	0.008	2.8961	145.1211
ASP_693@OD2	GLY_114@H	GLY_114@N	0.0078	2.8282	151.0401
ASP_444@HB2	GLU_74@HA	GLU_74@CA	0.0075	2.932	140.1817
ILE_658@HG21	GLN_174@HE21	GLN_174@NE2	0.0074	2.8413	143.9813
PRO_374@O	THR_168@HG1	THR_168@OG1	0.0074	2.793	162.0434
ALA_446@O	GLN_82@HE21	GLN_82@NE2	0.0074	2.8842	158.7513
GLY_660@HA2	TYR_173@HB2	TYR_173@CB	0.0073	2.9389	140.9048
LEU_662@O	GLN_166@HE22	GLN_166@NE2	0.0072	2.8471	154.1032
SER_441@HB2	GLU_74@H	GLU_74@N	0.0068	2.6708	142.1302
ALA_445@HB1	ALA_79@HA	ALA_79@CA	0.0068	2.9442	145.345
ASP_693@OD1	LYS_112@HZ2	LYS_112@NZ	0.0064	2.8094	154.5995
ASP_444@HB3	VAL_75@HA	VAL_75@CA	0.0062	2.9406	138.9447
LYS_694@HE2	SER_111@HA	SER_111@CA	0.0062	2.8984	143.8195
GLU_656@HG2	ASN_105@HD21	ASN_105@ND2	0.0061	2.7647	143.4448
LEU_691@HD23	ASN_107@HD21	ASN_107@ND2	0.0061	2.8335	148.0548
GLU_656@HG2	ASN_105@HD22	ASN_105@ND2	0.0059	2.7769	150.8676
LEU_440@HD23	ARG_76@HA	ARG_76@CA	0.0058	2.9436	146.6591
GLU_656@OE1	ASN_107@H	ASN_107@N	0.0057	2.8603	164.4997
SER_449@HB2	GLN_77@HB2	GLN_77@CB	0.0056	2.9403	143.2858
ARG_322@HH22	ARG_71@HH21	ARG_71@NH2	0.0054	2.9135	141.4983
LYS_652@O	ASN_105@HD21	ASN_105@ND2	0.0054	2.8489	148.7985
ARG_325@HH21	ARG_76@HH12	ARG_76@NH1	0.0052	2.9262	146.5059
LEU_691@HD22	ASN_107@HD21	ASN_107@ND2	0.0052	2.8361	148.742
ALA_690@O	LYS_112@HZ1	LYS_112@NZ	0.0052	2.8194	153.7032
TYR_695@HH	SER_162@HG	SER_162@OG	0.0051	2.8994	148.4591
SER_710@O	ASN_149@HD21	ASN_149@ND2	0.0051	2.8584	153.6397
GLN_670@HE22	GLN_166@HB3	GLN_166@CB	0.005	2.921	144.206
GLN_450@HE22	GLN_77@HE22	GLN_77@NE2	0.005	2.8928	149.5039
GLU_656@HB3	TYR_176@HH	TYR_176@OH	0.005	2.7949	143.903
LEU_662@HB2	THR_168@HB	THR_168@CB	0.005	2.9385	139.612

12.4.1.4. Determination of the protein-protein interface interactions of the (S protein-L-SIGN) and (S protein-CAT) complexes.

An interface area is usually defined as a region where two sets of proteins come in contact with each other. Surface residues are often characterized by extensive surface areas that are accessible to the available solvent. In order to determine the interface statistics for the (S protein-L-SIGN) and (S protein-CAT) complexes, we submitted the lowest energy structure extracted from the 100 ns MD simulation trajectory using the RMSD clustering algorithm to the PDBsum server. The interface statistics for both complexes have been shown in **Table 12.5.**

Table 12.5. *Protein-Protein interface interaction statistics for the S protein-L-SIGN and S protein-CAT complexes obtained from PDBsum server.*

Complex system	Chain	No. of interface residues	Interface area (Å^2)	No. of salt bridges	No. of disulphide bonds	No. of hydrogen bonds	No. of non-bonded contacts
S-protein-L-SIGN	S protein	14	807	2	-	12	103
	L-SIGN receptor	14	819				
S-protein- CAT	S protein	29	1803	4	-	25	236
	CAT receptor	31	1747				

The interface area shared by the S protein chain and the CAT chain in S protein-CAT complex was observed to be 1803 Å^2 and 1747 Å^2 respectively, while in the S protein-L-SIGN complex, the interface area shared by the S protein chain and the L-SIGN chain involved in the interaction was observed to be 807 Å^2 and 819 Å^2 respectively. Salt bridges, hydrogen bonds, and non-bonded contacts all played a role in stabilising both the (S protein-L-SIGN) and (S protein-CAT) complexes. From **Table 12.5**, we can see the presence of four salt bridges, two hundred and thirty-six non-bonded contacts and twenty-five hydrogen bonds at the interface of S protein and CAT in the S protein-CAT complex. However, at the interface of S protein and L-SIGN in the S protein-L-SIGN complex, we observed two salt bridges one hundred and three non-bonded contacts and twelve hydrogen bonds. An increase in the number of hydrogen bonds from twelve to twenty-five can be seen in the S protein-CAT complex. Overall, we see that the S protein-CAT complex has more intermolecular interactions and a larger common interface area shared by the S protein and CAT than the S protein-L-SIGN complex. Additionally, when compared our analysis with the results obtained for the S protein-ACE2 complex in our earlier studies and we found the number of intermolecular contacts and the interface area shared by S protein and receptors (CAT and L-SIGN) are higher. As a result, it can be concluded that the S protein-CAT complex had higher stability than the S protein-L-SIGN complex.

The residues that were involved in the interaction between the RBD of S protein and the receptors (L-SIGN and CAT) have been shown in **Figure 12.8A and 12.8B** respectively.

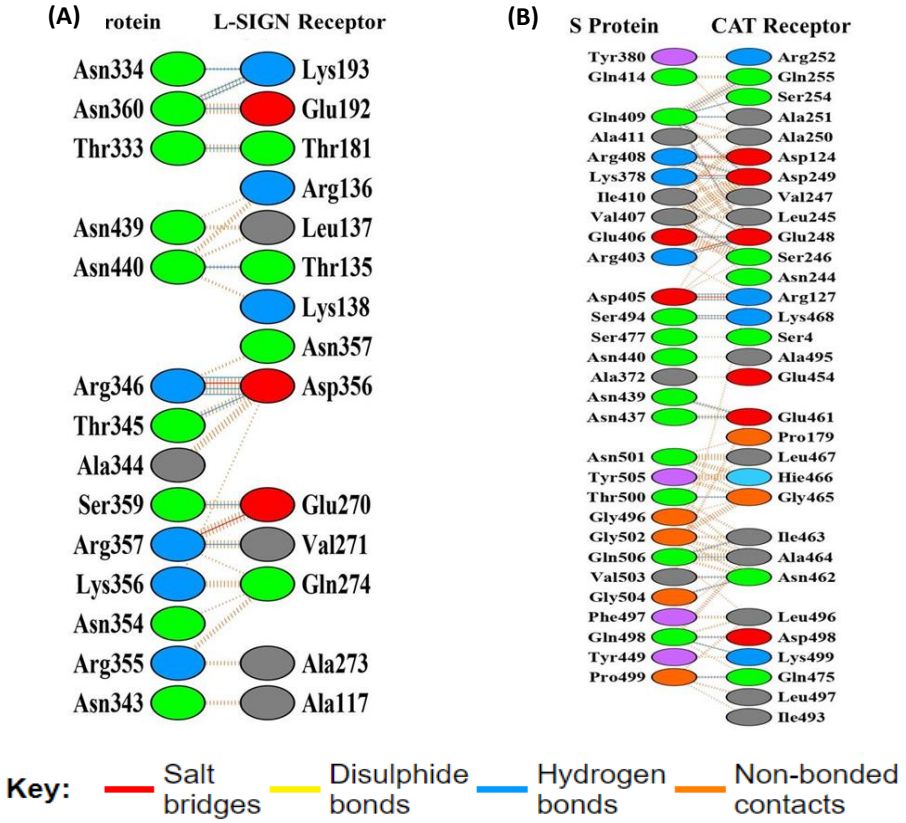

Figure 12.8. *Intermolecular interactions at residue level between* ***(A)*** *S protein-L-SIGN and* ***(B)*** *S protein-CAT complex.*

The detailed contributions of each interface residue stabilizing the (S protein-L-SIGN) and (S protein-CAT) complexes were analysed and are summarized in **Table 12.6, 12.7, 12.8 and 12.9, 12.10, 12.11**.

Table 12.6: *List of atom-atom interactions (Hydrogen bonds) across protein-ligand interface in Spike Protein (Chain A) and L-SIGN receptor (Chain B) complex from PDBsum server*

Spike Protein (Chain A)						Hydrogen bonds	*L-SIGN receptor (Chain B)*					
Sl.no.	Atom no.	Atom name	Res name	Res no.	Chain		Atom no.	Atom name	Res name	Res no.	Chain	Distance
1	13	OG1	THR	333	A	<-->	5945	OG1	THR	181	B	2.7
2	25	OD1	ASN	334	A	<-->	6127	NZ	LYS	193	B	2.74
3	177	N	THR	345	A	<-->	8681	OD2	ASP	356	B	2.93
4	191	N	ARG	346	A	<-->	8681	OD2	ASP	356	B	3.04
5	204	NE	ARG	346	A	<-->	8683	O	ASP	356	B	2.78
6	204	NE	ARG	346	A	<-->	8681	OD2	ASP	356	B	3.17
7	403	NH1	ARG	357	A	<-->	7393	O	VAL	271	B	2.75
8	437	OG	SER	359	A	<-->	7375	OE2	GLU	270	B	2.6
9	454	O	ASN	360	A	<-->	6127	NZ	LYS	193	B	2.83
10	449	OD1	ASN	360	A	<-->	6127	NZ	LYS	193	B	2.91

11	450	ND2	ASN	360	A	<-->	6108	OE2	GLU	192	B	2.87
12	1651	ND2	ASN	440	A	<-->	5184	O	THR	135	B	2.78

Table 12.7: *List of atom-atom interactions (non-bonded contacts) across protein-ligand interface in Spike Protein (Chain A) and L-SIGN receptor (Chain B) complex from PDBsum server*

Spike Protein (Chain A)						Non-bonded contacts	*L-SIGN receptor (Chain B)*					
Sl. No.	Atom no.	Atom name	Res name	Res no.	Chain		Atom no.	Atom name	Res name	Res no.	Chain	Distance
1	7	CB	THR	333	A	<-->	5945	OG1	THR	181	B	3.68
2	13	OG1	THR	333	A	<-->	5937	CA	THR	181	B	3.79
3	13	OG1	THR	333	A	<-->	5939	CB	THR	181	B	3.35
4	13	OG1	THR	333	A	<-->	5945	OG1	THR	181	B	2.7
5	13	OG1	THR	333	A	<-->	5941	CG2	THR	181	B	3.24
6	9	CG2	THR	333	A	<-->	5945	OG1	THR	181	B	3.71
7	25	OD1	ASN	334	A	<-->	6124	CE	LYS	193	B	3.48
8	25	OD1	ASN	334	A	<-->	6127	NZ	LYS	193	B	2.74
9	162	ND2	ASN	343	A	<-->	4886	C	ALA	117	B	3.77
10	162	ND2	ASN	343	A	<-->	4887	O	ALA	117	B	3.57
11	162	ND2	ASN	343	A	<-->	4882	CB	ALA	117	B	3.9
12	169	CA	ALA	344	A	<-->	8679	CG	ASP	356	B	3.89
13	169	CA	ALA	344	A	<-->	8680	OD1	ASP	356	B	3.84
14	169	CA	ALA	344	A	<-->	8681	OD2	ASP	356	B	3.86
15	175	C	ALA	344	A	<-->	8681	OD2	ASP	356	B	3.73
16	171	CB	ALA	344	A	<-->	8679	CG	ASP	356	B	3.79
17	171	CB	ALA	344	A	<-->	8681	OD2	ASP	356	B	3.68
18	177	N	THR	345	A	<-->	8679	CG	ASP	356	B	3.5
19	177	N	THR	345	A	<-->	8680	OD1	ASP	356	B	3.49
20	177	N	THR	345	A	<-->	8681	OD2	ASP	356	B	2.93
21	179	CA	THR	345	A	<-->	8681	OD2	ASP	356	B	3.62
22	189	C	THR	345	A	<-->	8681	OD2	ASP	356	B	3.77
23	181	CB	THR	345	A	<-->	8681	OD2	ASP	356	B	3.81
24	191	N	ARG	346	A	<-->	8681	OD2	ASP	356	B	3.04
25	195	CB	ARG	346	A	<-->	8683	O	ASP	356	B	3.8
26	198	CG	ARG	346	A	<-->	8683	O	ASP	356	B	3.82
27	201	CD	ARG	346	A	<-->	8683	O	ASP	356	B	3.79
28	204	NE	ARG	346	A	<-->	8682	C	ASP	356	B	3.66
29	204	NE	ARG	346	A	<-->	8683	O	ASP	356	B	2.78
30	204	NE	ARG	346	A	<-->	8681	OD2	ASP	356	B	3.17
31	206	CZ	ARG	346	A	<-->	8683	O	ASP	356	B	3.42
32	206	CZ	ARG	346	A	<-->	8681	OD2	ASP	356	B	3.39
33	206	CZ	ARG	346	A	<-->	8688	CB	ASN	357	B	3.88
34	207	NH1	ARG	346	A	<-->	8693	ND2	ASN	357	B	3.46

35	210	NH2	ARG	346	A	<-->	8682	C	ASP	356	B	3.63
36	210	NH2	ARG	346	A	<-->	8683	O	ASP	356	B	3.41
37	210	NH2	ARG	346	A	<-->	8679	CG	ASP	356	B	3.24
38	210	NH2	ARG	346	A	<-->	8680	OD1	ASP	356	B	3.42
39	210	NH2	ARG	346	A	<-->	8681	OD2	ASP	356	B	2.88
40	336	ND2	ASN	354	A	<-->	7432	CB	GLN	274	B	3.86
41	364	O	ARG	355	A	<-->	7422	CB	ALA	273	B	3.72
42	364	O	ARG	355	A	<-->	7428	N	GLN	274	B	3.42
43	364	O	ARG	355	A	<-->	7430	CA	GLN	274	B	3.83
44	364	O	ARG	355	A	<-->	7432	CB	GLN	274	B	3.42
45	364	O	ARG	355	A	<-->	7439	OE1	GLN	274	B	3.61
46	345	CB	ARG	355	A	<-->	7422	CB	ALA	273	B	3.81
47	348	CG	ARG	355	A	<-->	7422	CB	ALA	273	B	3.88
48	367	CA	LYS	356	A	<-->	7438	CD	GLN	274	B	3.83
49	367	CA	LYS	356	A	<-->	7439	OE1	GLN	274	B	3.19
50	369	CB	LYS	356	A	<-->	7438	CD	GLN	274	B	3.71
51	369	CB	LYS	356	A	<-->	7439	OE1	GLN	274	B	3.53
52	372	CG	LYS	356	A	<-->	7438	CD	GLN	274	B	3.83
53	381	NZ	LYS	356	A	<-->	8676	CB	ASP	356	B	3.79
54	387	N	ARG	357	A	<-->	7439	OE1	GLN	274	B	3.76
55	397	CD	ARG	357	A	<-->	7393	O	VAL	271	B	3.15
56	400	NE	ARG	357	A	<-->	7370	CG	GLU	270	B	3.71
57	400	NE	ARG	357	A	<-->	7373	CD	GLU	270	B	3.68
58	400	NE	ARG	357	A	<-->	7393	O	VAL	271	B	3.86
59	402	CZ	ARG	357	A	<-->	7370	CG	GLU	270	B	3.36
60	402	CZ	ARG	357	A	<-->	7373	CD	GLU	270	B	3.69
61	402	CZ	ARG	357	A	<-->	7393	O	VAL	271	B	3.67
62	403	NH1	ARG	357	A	<-->	7370	CG	GLU	270	B	3.33
63	403	NH1	ARG	357	A	<-->	7378	N	VAL	271	B	3.56
64	403	NH1	ARG	357	A	<-->	7392	C	VAL	271	B	3.73
65	403	NH1	ARG	357	A	<-->	7393	O	VAL	271	B	2.75
66	406	NH2	ARG	357	A	<-->	7370	CG	GLU	270	B	3.69
67	406	NH2	ARG	357	A	<-->	7373	CD	GLU	270	B	3.85
68	406	NH2	ARG	357	A	<-->	7375	OE2	GLU	270	B	3.74
69	434	CB	SER	359	A	<-->	7373	CD	GLU	270	B	3.44
70	434	CB	SER	359	A	<-->	7374	OE1	GLU	270	B	3
71	434	CB	SER	359	A	<-->	7375	OE2	GLU	270	B	3.13
72	437	OG	SER	359	A	<-->	7373	CD	GLU	270	B	3.37
73	437	OG	SER	359	A	<-->	7374	OE1	GLU	270	B	3.42
74	437	OG	SER	359	A	<-->	7375	OE2	GLU	270	B	2.6
75	453	C	ASN	360	A	<-->	6127	NZ	LYS	193	B	3.67
76	454	O	ASN	360	A	<-->	6127	NZ	LYS	193	B	2.83
77	448	CG	ASN	360	A	<-->	6108	OE2	GLU	192	B	3.73
78	448	CG	ASN	360	A	<-->	6127	NZ	LYS	193	B	3.54

79	449	OD1	ASN	360	A	<-->	6100	CB	GLU	192	B	3.64
80	449	OD1	ASN	360	A	<-->	6103	CG	GLU	192	B	3.67
81	449	OD1	ASN	360	A	<-->	6108	OE2	GLU	192	B	3.79
82	449	OD1	ASN	360	A	<-->	6121	CD	LYS	193	B	3.84
83	449	OD1	ASN	360	A	<-->	6124	CE	LYS	193	B	3.46
84	449	OD1	ASN	360	A	<-->	6127	NZ	LYS	193	B	2.91
85	450	ND2	ASN	360	A	<-->	6103	CG	GLU	192	B	3.86
86	450	ND2	ASN	360	A	<-->	6106	CD	GLU	192	B	3.28
87	450	ND2	ASN	360	A	<-->	6107	OE1	GLU	192	B	3.9
88	450	ND2	ASN	360	A	<-->	6108	OE2	GLU	192	B	2.87
89	1640	C	ASN	439	A	<-->	5208	O	ARG	136	B	3.8
90	1641	O	ASN	439	A	<-->	5211	CA	LEU	137	B	3.86
91	1641	O	ASN	439	A	<-->	5227	O	LEU	137	B	3.71
92	1637	ND2	ASN	439	A	<-->	5213	CB	LEU	137	B	3.62
93	1642	N	ASN	440	A	<-->	5208	O	ARG	136	B	3.19
94	1644	CA	ASN	440	A	<-->	5208	O	ARG	136	B	3.76
95	1644	CA	ASN	440	A	<-->	5211	CA	LEU	137	B	3.89
96	1644	CA	ASN	440	A	<-->	5226	C	LEU	137	B	3.84
97	1655	O	ASN	440	A	<-->	5249	O	LYS	138	B	3.56
98	1646	CB	ASN	440	A	<-->	5184	O	THR	135	B	3.11
99	1646	CB	ASN	440	A	<-->	5207	C	ARG	136	B	3.65
100	1646	CB	ASN	440	A	<-->	5208	O	ARG	136	B	3.32
101	1646	CB	ASN	440	A	<-->	5249	O	LYS	138	B	3.67
102	1649	CG	ASN	440	A	<-->	5184	O	THR	135	B	3.41
103	1651	ND2	ASN	440	A	<-->	5184	O	THR	135	B	2.78

Table 12.8. *List of atom-atom interactions (Salt bridges) across protein-ligand interface in Spike Protein (Chain A) and L-SIGN receptor (Chain B) complex from PDBsum server*

Spike Protein (Chain A)							*L-SIGN receptor (Chain B)*					
Sl.no.	Atom no.	Atom name	Res name	Res no.	Chain	Salt bridges	Atom no.	Atom name	Res name	Res no.	Chain	Distance
1	210	NH2	ARG	346	A	<-->	8681	OD2	ASP	356	B	2.88
2	406	NH2	ARG	357	A	<-->	7374	OE1	GLU	270	B	3.74

Table 12.9: *List of atom-atom interactions (Hydrogen bonds) across protein-ligand interface in Spike Protein (Chain A) and CAT receptor (Chain B) complex from PDBsum server*

Spike Protein (Chain A)							*CAT receptor (Chain B)*					
Sl.no.	Atom no.	Atom name	Res name	Res no.	Chain	Hydrogen bonds	Atom no.	Atom name	Res name	Res no.	Chain	Distance
1	717	NZ	LYS	378	A	<-->	6897	OD2	ASP	249	B	2.93
2	1104	NH2	ARG	403	A	<-->	6884	OE1	GLU	248	B	2.79

3	1124	OD1	ASP	405	A	<-->	4941	NH1	ARG	127	B	2.91
4	1125	OD2	ASP	405	A	<-->	4944	NH2	ARG	127	B	2.7
5	1142	O	GLU	406	A	<-->	6873	N	GLU	248	B	2.78
6	1158	O	VAL	407	A	<-->	6846	N	SER	246	B	2.85
7	1159	N	ARG	408	A	<-->	6899	O	ASP	249	B	2.78
8	1183	N	GLN	409	A	<-->	6887	O	GLU	248	B	3.09
9	1183	N	GLN	409	A	<-->	6899	O	ASP	249	B	2.96
10	1199	O	GLN	409	A	<-->	6910	N	ALA	251	B	3.02
11	1194	OE1	GLN	409	A	<-->	6970	OG	SER	254	B	3.01
12	1195	NE2	GLN	409	A	<-->	6985	OE1	GLN	255	B	2.79
13	1200	N	ILE	410	A	<-->	6887	O	GLU	248	B	3.09
14	1615	ND2	ASN	437	A	<-->	10248	OE1	GLU	461	B	3.24
15	1640	ND2	ASN	439	A	<-->	10248	OE1	GLU	461	B	2.82
16	2509	O	SER	494	A	<-->	10354	NZ	LYS	468	B	2.95
17	2506	OG	SER	494	A	<-->	10354	NZ	LYS	468	B	2.71
18	2570	NE2	GLN	498	A	<-->	10839	O	ASP	498	B	2.84
19	2570	NE2	GLN	498	A	<-->	10861	O	LYS	499	B	2.97
20	2588	O	PRO	499	A	<-->	10469	NE2	GLN	475	B	2.98
21	2599	OG1	THR	500	A	<-->	10295	N	GLY	465	B	2.8
22	2624	N	VAL	503	A	<-->	10265	O	ASN	462	B	2.96
23	2640	N	GLY	504	A	<-->	10260	OD1	ASN	462	B	2.87
24	2679	OE1	GLN	506	A	<-->	10266	N	ILE	463	B	2.78
25	2679	OE1	GLN	506	A	<-->	10285	N	ALA	464	B	2.97

Table 12.10. *List of atom-atom interactions (non-bonded contacts) across protein-ligand interface in Spike Protein (Chain A) and CAT receptor (Chain B) complex from PDBsum server.*

Spike Protein (Chain A)							*CAT receptor (Chain B)*					
Sl. no	Atom no.	Atom name	Res name	Res no.	Chain	Non-bonded contacts	Atom no.	Atom name	Res name	Res no.	Chain	Distance
1	624	O	ALA	372	A	<-->	10117	OE2	GLU	454	B	3.76
2	717	NZ	LYS	378	A	<-->	6897	OD2	ASP	249	B	2.93
3	741	CD1	TYR	380	A	<-->	6939	NH2	ARG	252	B	3.48
4	743	CE1	TYR	380	A	<-->	6939	NH2	ARG	252	B	3.65
5	746	OH	TYR	380	A	<-->	6904	CB	ALA	250	B	3.35
6	1098	NE	ARG	403	A	<-->	4944	NH2	ARG	127	B	3.57
7	1100	CZ	ARG	403	A	<-->	6884	OE1	GLU	248	B	3.87
8	1104	NH2	ARG	403	A	<-->	6880	CG	GLU	248	B	3.63
9	1104	NH2	ARG	403	A	<-->	6883	CD	GLU	248	B	3.54
10	1104	NH2	ARG	403	A	<-->	6884	OE1	GLU	248	B	2.79
11	1127	O	ASP	405	A	<-->	6892	CB	ASP	249	B	3.43
12	1120	CB	ASP	405	A	<-->	6856	O	SER	246	B	3.66
13	1120	CB	ASP	405	A	<-->	6877	CB	GLU	248	B	3.51

14	1123	CG	ASP	405	A	<-->	4941	NH1	ARG	127	B	3.42
15	1123	CG	ASP	405	A	<-->	4944	NH2	ARG	127	B	3.56
16	1124	OD1	ASP	405	A	<-->	4940	CZ	ARG	127	B	3.81
17	1124	OD1	ASP	405	A	<-->	4941	NH1	ARG	127	B	2.91
18	1124	OD1	ASP	405	A	<-->	4944	NH2	ARG	127	B	3.76
19	1125	OD2	ASP	405	A	<-->	4940	CZ	ARG	127	B	3.48
20	1125	OD2	ASP	405	A	<-->	4941	NH1	ARG	127	B	3.32
21	1125	OD2	ASP	405	A	<-->	4944	NH2	ARG	127	B	2.7
22	1128	N	GLU	406	A	<-->	6856	O	SER	246	B	3.78
23	1128	N	GLU	406	A	<-->	6850	CB	SER	246	B	3.77
24	1130	CA	GLU	406	A	<-->	6850	CB	SER	246	B	3.76
25	1130	CA	GLU	406	A	<-->	6892	CB	ASP	249	B	3.69
26	1141	C	GLU	406	A	<-->	6850	CB	SER	246	B	3.57
27	1141	C	GLU	406	A	<-->	6888	N	ASP	249	B	3.37
28	1141	C	GLU	406	A	<-->	6892	CB	ASP	249	B	3.65
29	1142	O	GLU	406	A	<-->	6846	N	SER	246	B	3.82
30	1142	O	GLU	406	A	<-->	6848	CA	SER	246	B	3.54
31	1142	O	GLU	406	A	<-->	6855	C	SER	246	B	3.09
32	1142	O	GLU	406	A	<-->	6856	O	SER	246	B	3.15
33	1142	O	GLU	406	A	<-->	6850	CB	SER	246	B	3.44
34	1142	O	GLU	406	A	<-->	6857	N	VAL	247	B	3.55
35	1142	O	GLU	406	A	<-->	6871	C	VAL	247	B	3.87
36	1142	O	GLU	406	A	<-->	6873	N	GLU	248	B	2.78
37	1142	O	GLU	406	A	<-->	6875	CA	GLU	248	B	3.48
38	1142	O	GLU	406	A	<-->	6886	C	GLU	248	B	3.59
39	1142	O	GLU	406	A	<-->	6877	CB	GLU	248	B	3.9
40	1142	O	GLU	406	A	<-->	6888	N	ASP	249	B	3.09
41	1132	CB	GLU	406	A	<-->	6850	CB	SER	246	B	3.52
42	1143	N	VAL	407	A	<-->	6888	N	ASP	249	B	3.63
43	1143	N	VAL	407	A	<-->	6890	CA	ASP	249	B	3.89
44	1143	N	VAL	407	A	<-->	6898	C	ASP	249	B	3.84
45	1143	N	VAL	407	A	<-->	6899	O	ASP	249	B	3.89
46	1143	N	VAL	407	A	<-->	6892	CB	ASP	249	B	3.71
47	1145	CA	VAL	407	A	<-->	6898	C	ASP	249	B	3.7
48	1145	CA	VAL	407	A	<-->	6899	O	ASP	249	B	3.29
49	1157	C	VAL	407	A	<-->	6888	N	ASP	249	B	3.82
50	1157	C	VAL	407	A	<-->	6899	O	ASP	249	B	3.46
51	1158	O	VAL	407	A	<-->	6829	CA	LEU	245	B	3.66
52	1158	O	VAL	407	A	<-->	6844	C	LEU	245	B	3.69
53	1158	O	VAL	407	A	<-->	6831	CB	LEU	245	B	3.83
54	1158	O	VAL	407	A	<-->	6846	N	SER	246	B	2.85
55	1158	O	VAL	407	A	<-->	6848	CA	SER	246	B	3.72
56	1158	O	VAL	407	A	<-->	6855	C	SER	246	B	3.75
57	1158	O	VAL	407	A	<-->	6857	N	VAL	247	B	3.42

58	1149	CG1	VAL	407	A	<-->	6909	O	ALA	250	B	3.82
59	1153	CG2	VAL	407	A	<-->	6826	O	ASN	244	B	3.44
60	1153	CG2	VAL	407	A	<-->	6846	N	SER	246	B	3.78
61	1159	N	ARG	408	A	<-->	6886	C	GLU	248	B	3.53
62	1159	N	ARG	408	A	<-->	6887	O	GLU	248	B	3.71
63	1159	N	ARG	408	A	<-->	6888	N	ASP	249	B	3.58
64	1159	N	ARG	408	A	<-->	6898	C	ASP	249	B	3.75
65	1159	N	ARG	408	A	<-->	6899	O	ASP	249	B	2.78
66	1161	CA	ARG	408	A	<-->	6899	O	ASP	249	B	3.72
67	1181	C	ARG	408	A	<-->	6887	O	GLU	248	B	3.88
68	1181	C	ARG	408	A	<-->	6899	O	ASP	249	B	3.57
69	1182	O	ARG	408	A	<-->	6914	CB	ALA	251	B	3.76
70	1163	CB	ARG	408	A	<-->	6859	CA	VAL	247	B	3.8
71	1163	CB	ARG	408	A	<-->	6871	C	VAL	247	B	3.66
72	1163	CB	ARG	408	A	<-->	6873	N	GLU	248	B	3.71
73	1163	CB	ARG	408	A	<-->	6887	O	GLU	248	B	3.85
74	1172	NE	ARG	408	A	<-->	4892	OD2	ASP	124	B	3.73
75	1174	CZ	ARG	408	A	<-->	4892	OD2	ASP	124	B	3.58
76	1178	NH2	ARG	408	A	<-->	4887	CB	ASP	124	B	3.59
77	1178	NH2	ARG	408	A	<-->	4890	CG	ASP	124	B	3.46
78	1178	NH2	ARG	408	A	<-->	4892	OD2	ASP	124	B	2.73
79	1183	N	GLN	409	A	<-->	6887	O	GLU	248	B	3.09
80	1183	N	GLN	409	A	<-->	6899	O	ASP	249	B	2.96
81	1185	CA	GLN	409	A	<-->	6887	O	GLU	248	B	3.9
82	1185	CA	GLN	409	A	<-->	6899	O	ASP	249	B	3.8
83	1198	C	GLN	409	A	<-->	6887	O	GLU	248	B	3.84
84	1198	C	GLN	409	A	<-->	6899	O	ASP	249	B	3.6
85	1198	C	GLN	409	A	<-->	6910	N	ALA	251	B	3.89
86	1199	O	GLN	409	A	<-->	6899	O	ASP	249	B	3.87
87	1199	O	GLN	409	A	<-->	6902	CA	ALA	250	B	3.43
88	1199	O	GLN	409	A	<-->	6908	C	ALA	250	B	3.62
89	1199	O	GLN	409	A	<-->	6910	N	ALA	251	B	3.02
90	1199	O	GLN	409	A	<-->	6986	NE2	GLN	255	B	3.28
91	1193	CD	GLN	409	A	<-->	6985	OE1	GLN	255	B	3.53
92	1193	CD	GLN	409	A	<-->	6986	NE2	GLN	255	B	3.36
93	1194	OE1	GLN	409	A	<-->	6967	CB	SER	254	B	3.61
94	1194	OE1	GLN	409	A	<-->	6970	OG	SER	254	B	3.01
95	1194	OE1	GLN	409	A	<-->	6984	CD	GLN	255	B	3.69
96	1194	OE1	GLN	409	A	<-->	6985	OE1	GLN	255	B	3.41
97	1194	OE1	GLN	409	A	<-->	6986	NE2	GLN	255	B	3.27
98	1195	NE2	GLN	409	A	<-->	6984	CD	GLN	255	B	3.42
99	1195	NE2	GLN	409	A	<-->	6985	OE1	GLN	255	B	2.79
100	1195	NE2	GLN	409	A	<-->	6986	NE2	GLN	255	B	3.07
101	1200	N	ILE	410	A	<-->	6887	O	GLU	248	B	3.09

102	1200	N	ILE	410	A	<-->	6899	O	ASP	249	B	3.67
103	1217	C	ILE	410	A	<-->	6900	N	ALA	250	B	3.89
104	1217	C	ILE	410	A	<-->	6902	CA	ALA	250	B	3.63
105	1218	O	ILE	410	A	<-->	6890	CA	ASP	249	B	3.67
106	1218	O	ILE	410	A	<-->	6898	C	ASP	249	B	3.54
107	1218	O	ILE	410	A	<-->	6896	OD1	ASP	249	B	3.74
108	1218	O	ILE	410	A	<-->	6900	N	ALA	250	B	3.07
109	1218	O	ILE	410	A	<-->	6902	CA	ALA	250	B	3.16
110	1218	O	ILE	410	A	<-->	6904	CB	ALA	250	B	3.52
111	1206	CG2	ILE	410	A	<-->	6887	O	GLU	248	B	3.51
112	1206	CG2	ILE	410	A	<-->	6885	OE2	GLU	248	B	3.44
113	1221	CA	ALA	411	A	<-->	6904	CB	ALA	250	B	3.62
114	1223	CB	ALA	411	A	<-->	6902	CA	ALA	250	B	3.89
115	1223	CB	ALA	411	A	<-->	6904	CB	ALA	250	B	3.45
116	1262	NE2	GLN	414	A	<-->	6984	CD	GLN	255	B	3.84
117	1262	NE2	GLN	414	A	<-->	6985	OE1	GLN	255	B	3.82
118	1262	NE2	GLN	414	A	<-->	6986	NE2	GLN	255	B	3.6
119	1613	CG	ASN	437	A	<-->	10248	OE1	GLU	461	B	3.89
120	1614	OD1	ASN	437	A	<-->	10248	OE1	GLU	461	B	3.69
121	1615	ND2	ASN	437	A	<-->	10244	CG	GLU	461	B	3.5
122	1615	ND2	ASN	437	A	<-->	10247	CD	GLU	461	B	3.73
123	1615	ND2	ASN	437	A	<-->	10248	OE1	GLU	461	B	3.24
124	1635	CB	ASN	439	A	<-->	10248	OE1	GLU	461	B	3.35
125	1638	CG	ASN	439	A	<-->	10248	OE1	GLU	461	B	3.56
126	1640	ND2	ASN	439	A	<-->	10247	CD	GLU	461	B	3.82
127	1640	ND2	ASN	439	A	<-->	10248	OE1	GLU	461	B	2.82
128	1654	ND2	ASN	440	A	<-->	10784	CB	ALA	495	B	3.33
129	1782	CE2	TYR	449	A	<-->	10850	CD	LYS	499	B	3.83
130	2263	OG	SER	477	A	<-->	3054	CB	SER	4	B	3.77
131	2508	C	SER	494	A	<-->	10354	NZ	LYS	468	B	3.69
132	2509	O	SER	494	A	<-->	10354	NZ	LYS	468	B	2.95
133	2503	CB	SER	494	A	<-->	10354	NZ	LYS	468	B	3.76
134	2506	OG	SER	494	A	<-->	10351	CE	LYS	468	B	3.31
135	2506	OG	SER	494	A	<-->	10354	NZ	LYS	468	B	2.71
136	2533	CA	GLY	496	A	<-->	10301	O	GLY	465	B	3.32
137	2536	C	GLY	496	A	<-->	10289	CB	ALA	464	B	3.67
138	2537	O	GLY	496	A	<-->	10289	CB	ALA	464	B	3.88
139	2538	N	PHE	497	A	<-->	10289	CB	ALA	464	B	3.74
140	2556	C	PHE	497	A	<-->	10799	CD1	LEU	496	B	3.57
141	2557	O	PHE	497	A	<-->	10808	O	LEU	496	B	3.07
142	2557	O	PHE	497	A	<-->	10799	CD1	LEU	496	B	3.29
143	2558	N	GLN	498	A	<-->	10289	CB	ALA	464	B	3.69
144	2560	CA	GLN	498	A	<-->	10808	O	LEU	496	B	3.59
145	2573	C	GLN	498	A	<-->	10289	CB	ALA	464	B	3.76

146	2574	O	GLN	498	A	<-->	10287	CA	ALA	464	B	3.4
147	2574	O	GLN	498	A	<-->	10289	CB	ALA	464	B	3.05
148	2562	CB	GLN	498	A	<-->	10469	NE2	GLN	475	B	3.74
149	2565	CG	GLN	498	A	<-->	10808	O	LEU	496	B	3.58
150	2565	CG	GLN	498	A	<-->	10839	O	ASP	498	B	3.24
151	2568	CD	GLN	498	A	<-->	10839	O	ASP	498	B	3.48
152	2570	NE2	GLN	498	A	<-->	10839	O	ASP	498	B	2.84
153	2570	NE2	GLN	498	A	<-->	10860	C	LYS	499	B	3.82
154	2570	NE2	GLN	498	A	<-->	10861	O	LYS	499	B	2.97
155	2588	O	PRO	499	A	<-->	10464	CG	GLN	475	B	3.57
156	2588	O	PRO	499	A	<-->	10467	CD	GLN	475	B	3.74
157	2588	O	PRO	499	A	<-->	10469	NE2	GLN	475	B	2.98
158	2579	CG	PRO	499	A	<-->	10754	CG1	ILE	493	B	3.64
159	2576	CD	PRO	499	A	<-->	10808	O	LEU	496	B	3.82
160	2576	CD	PRO	499	A	<-->	10797	CG	LEU	496	B	3.84
161	2576	CD	PRO	499	A	<-->	10809	N	LEU	497	B	3.85
162	2576	CD	PRO	499	A	<-->	10811	CA	LEU	497	B	3.83
163	2589	N	THR	500	A	<-->	10284	O	ILE	463	B	3.58
164	2602	O	THR	500	A	<-->	10284	O	ILE	463	B	3.81
165	2599	OG1	THR	500	A	<-->	10287	CA	ALA	464	B	3.32
166	2599	OG1	THR	500	A	<-->	10293	C	ALA	464	B	3.56
167	2599	OG1	THR	500	A	<-->	10295	N	GLY	465	B	2.8
168	2599	OG1	THR	500	A	<-->	10297	CA	GLY	465	B	3.64
169	2595	CG2	THR	500	A	<-->	10337	O	LEU	467	B	3.8
170	2607	CB	ASN	501	A	<-->	5785	CG	PRO	179	B	3.79
171	2607	CB	ASN	501	A	<-->	10328	CD1	LEU	467	B	3.8
172	2610	CG	ASN	501	A	<-->	10310	ND1	HIE	466	B	3.84
173	2610	CG	ASN	501	A	<-->	10326	CG	LEU	467	B	3.8
174	2610	CG	ASN	501	A	<-->	10328	CD1	LEU	467	B	3.44
175	2611	OD1	ASN	501	A	<-->	10297	CA	GLY	465	B	3.54
176	2611	OD1	ASN	501	A	<-->	10300	C	GLY	465	B	3.75
177	2611	OD1	ASN	501	A	<-->	10302	N	HIE	466	B	3.54
178	2611	OD1	ASN	501	A	<-->	10310	ND1	HIE	466	B	3.81
179	2611	OD1	ASN	501	A	<-->	10319	N	LEU	467	B	3.59
180	2611	OD1	ASN	501	A	<-->	10323	CB	LEU	467	B	3.63
181	2611	OD1	ASN	501	A	<-->	10326	CG	LEU	467	B	3.57
182	2611	OD1	ASN	501	A	<-->	10328	CD1	LEU	467	B	3.52
183	2612	ND2	ASN	501	A	<-->	10310	ND1	HIE	466	B	3.02
184	2612	ND2	ASN	501	A	<-->	10311	CE1	HIE	466	B	3.27
185	2617	N	GLY	502	A	<-->	10284	O	ILE	463	B	3.61
186	2617	N	GLY	502	A	<-->	10293	C	ALA	464	B	3.87
187	2617	N	GLY	502	A	<-->	10295	N	GLY	465	B	3.58
188	2617	N	GLY	502	A	<-->	10297	CA	GLY	465	B	3.28
189	2619	CA	GLY	502	A	<-->	10265	O	ASN	462	B	3.33

190	2619	CA	GLY	502	A	<-->	10283	C	ILE	463	B	3.88
191	2619	CA	GLY	502	A	<-->	10284	O	ILE	463	B	3.41
192	2619	CA	GLY	502	A	<-->	10293	C	ALA	464	B	3.64
193	2619	CA	GLY	502	A	<-->	10294	O	ALA	464	B	3.59
194	2619	CA	GLY	502	A	<-->	10295	N	GLY	465	B	3.81
195	2619	CA	GLY	502	A	<-->	10297	CA	GLY	465	B	3.63
196	2622	C	GLY	502	A	<-->	10265	O	ASN	462	B	3.63
197	2622	C	GLY	502	A	<-->	10294	O	ALA	464	B	3.84
198	2622	C	GLY	502	A	<-->	10297	CA	GLY	465	B	3.81
199	2623	O	GLY	502	A	<-->	10297	CA	GLY	465	B	3.68
200	2624	N	VAL	503	A	<-->	10264	C	ASN	462	B	3.82
201	2624	N	VAL	503	A	<-->	10265	O	ASN	462	B	2.96
202	2638	C	VAL	503	A	<-->	10260	OD1	ASN	462	B	3.83
203	2630	CG1	VAL	503	A	<-->	4935	CD	ARG	127	B	3.81
204	2640	N	GLY	504	A	<-->	10259	CG	ASN	462	B	3.85
205	2640	N	GLY	504	A	<-->	10260	OD1	ASN	462	B	2.87
206	2642	CA	GLY	504	A	<-->	10260	OD1	ASN	462	B	3.56
207	2654	CG	TYR	505	A	<-->	10300	C	GLY	465	B	3.81
208	2654	CG	TYR	505	A	<-->	10302	N	HIE	466	B	3.68
209	2664	CD2	TYR	505	A	<-->	10300	C	GLY	465	B	3.24
210	2664	CD2	TYR	505	A	<-->	10301	O	GLY	465	B	3.25
211	2664	CD2	TYR	505	A	<-->	10302	N	HIE	466	B	3.3
212	2664	CD2	TYR	505	A	<-->	10304	CA	HIE	466	B	3.43
213	2662	CE2	TYR	505	A	<-->	10301	O	GLY	465	B	3.83
214	2662	CE2	TYR	505	A	<-->	10302	N	HIE	466	B	3.88
215	2662	CE2	TYR	505	A	<-->	10304	CA	HIE	466	B	3.43
216	2662	CE2	TYR	505	A	<-->	10306	CB	HIE	466	B	3.79
217	2659	CZ	TYR	505	A	<-->	10306	CB	HIE	466	B	3.86
218	2675	CG	GLN	506	A	<-->	10294	O	ALA	464	B	3.34
219	2675	CG	GLN	506	A	<-->	10289	CB	ALA	464	B	3.73
220	2678	CD	GLN	506	A	<-->	10285	N	ALA	464	B	3.48
221	2678	CD	GLN	506	A	<-->	10294	O	ALA	464	B	3.87
222	2678	CD	GLN	506	A	<-->	10289	CB	ALA	464	B	3.6
223	2679	OE1	GLN	506	A	<-->	10239	CA	GLU	461	B	3.86
224	2679	OE1	GLN	506	A	<-->	10250	C	GLU	461	B	3.65
225	2679	OE1	GLN	506	A	<-->	10252	N	ASN	462	B	3.46
226	2679	OE1	GLN	506	A	<-->	10254	CA	ASN	462	B	3.81
227	2679	OE1	GLN	506	A	<-->	10264	C	ASN	462	B	3.57
228	2679	OE1	GLN	506	A	<-->	10266	N	ILE	463	B	2.78
229	2679	OE1	GLN	506	A	<-->	10268	CA	ILE	463	B	3.63
230	2679	OE1	GLN	506	A	<-->	10283	C	ILE	463	B	3.73
231	2679	OE1	GLN	506	A	<-->	10272	CG2	ILE	463	B	3.31
232	2679	OE1	GLN	506	A	<-->	10285	N	ALA	464	B	2.97
233	2679	OE1	GLN	506	A	<-->	10287	CA	ALA	464	B	3.85

234	2679	OE1	GLN	506	A	<-->	10294	O	ALA	464	B	3.73
235	2680	NE2	GLN	506	A	<-->	10289	CB	ALA	464	B	3.72
236	2680	NE2	GLN	506	A	<-->	10799	CD1	LEU	496	B	3.9

Table 12.11. *List of atom-atom interactions (Salt bridges) across protein-ligand interface in Spike Protein (Chain A) and CAT receptor (Chain B) complex from PDBsum server.*

Spike Protein (Chain A)						Salt bridges	*CAT receptor (Chain B)*					
Sl.no.	Atom no.	Atom name	Res name	Res no.	Chain		Atom no.	Atom name	Res name	Res no.	Chain	Distance
1	717	NZ	LYS	378	A	<-->	6896	OD1	ASP	249	B	2.93
2	1104	NH2	ARG	403	A	<-->	6884	OE1	GLU	248	B	2.79
3	1124	OD1	ASP	405	A	<-->	4944	NH2	ARG	127	B	2.7
4	1175	NH1	ARG	408	A	<-->	4891	OD1	ASP	124	B	2.73

12.4.1.5. Binding Free energy.

HawkDock, a web server to predict the BFE and analyse the protein-protein complex based on computational docking and Generalized Born surface area continuum solvation (MM/GBSA) meth ods, was used to calculate the binding free energies of the (S protein-L-SIGN) and (S protein-CAT) complexes. The bind ing free energies determined for the (S protein-L-SIGN) and (S protein-CAT) complexes along with the energy terms, were summarized in **Table 12.12**. From Table 12.12, it can be seen that S protein-CAT complex (ΔG_{bind}= -39.49 kcal/mol) was energetically more favourable than the S protein-L-SIGN complex (ΔG_{bind} = -37.20 kcal/ mol). Analysing Table 12.12, we observed that all the derived components (VDW, ELE, GB,SA) from the BFE analysis significantly contributed to the binding of S protein and receptors (L-SIGN and CAT).

Table 12.12. *Binding free energies (kcal/mol) and its derived components of S protein-L-SIGN and S protein-CAT complexes obtained using HawkDock server.*

Components	**S protein-L-SIGN complex (kcal/mol)**	**S protein-CAT complex (kcal/mol)**
VDW	-77.74	-113.38
ELE	-404.11	-219.97
GB	457.84	309.66
SA	-11.1	-15.8
Total ($\Delta G_{binding}$)	**-35.11**	**-39.49**

VDW = van der Waals contribution; ELE = electrostatic energy; GB = the electrostatic contribution to the polar solvation free energy, SA= Surface Area and BFE ($\Delta G_{binding}$).

12.4.1.6. Per residue energy decomposition (PRED) analysis

PRED values were calculated in order to get insight into how each individual amino acid residue contributed to the overall PPI of the (S protein-L-SIGN) and (S protein-CAT) complexes. **Figure 12.9 and 12.10** shows the top ten residues contributing to the binding free energy with the most negative energy values for the S protein-L-SIGN and S protein-CAT complex, respectively. The major binding energy contributions for S protein-L-SIGN come from the residues ARG375, ILE468, ARG346, TRP353, ASP467, PHE464, THR470, TYR351, TYR447, LEU452 while in S protein-CAT come from the residues ARG346, LYS386, SER373, ASN360, ASN440, LEU441, THR345, ALA344, ASN334, ILE486.

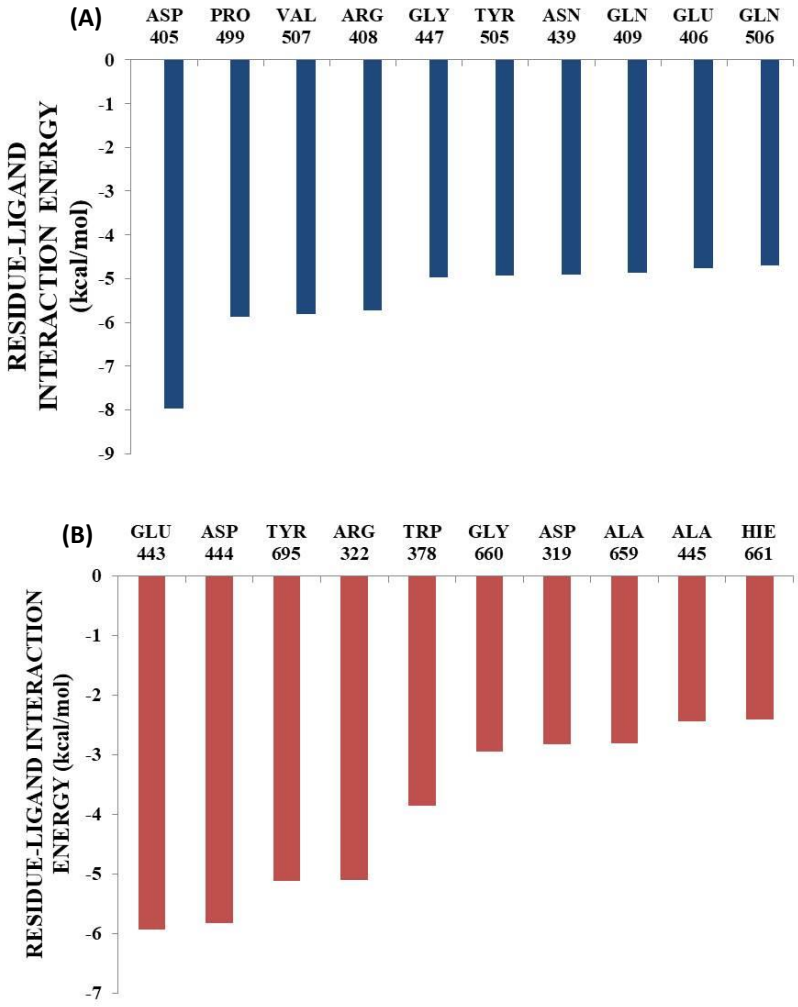

Figure 12.9. *Decomposition of binding free energy (kcal/mol) on per residue basis for* ***(A)*** *SPIKE* ***(B)*** *L-SIGN receptor of the S protein-L-SIGN complex.*

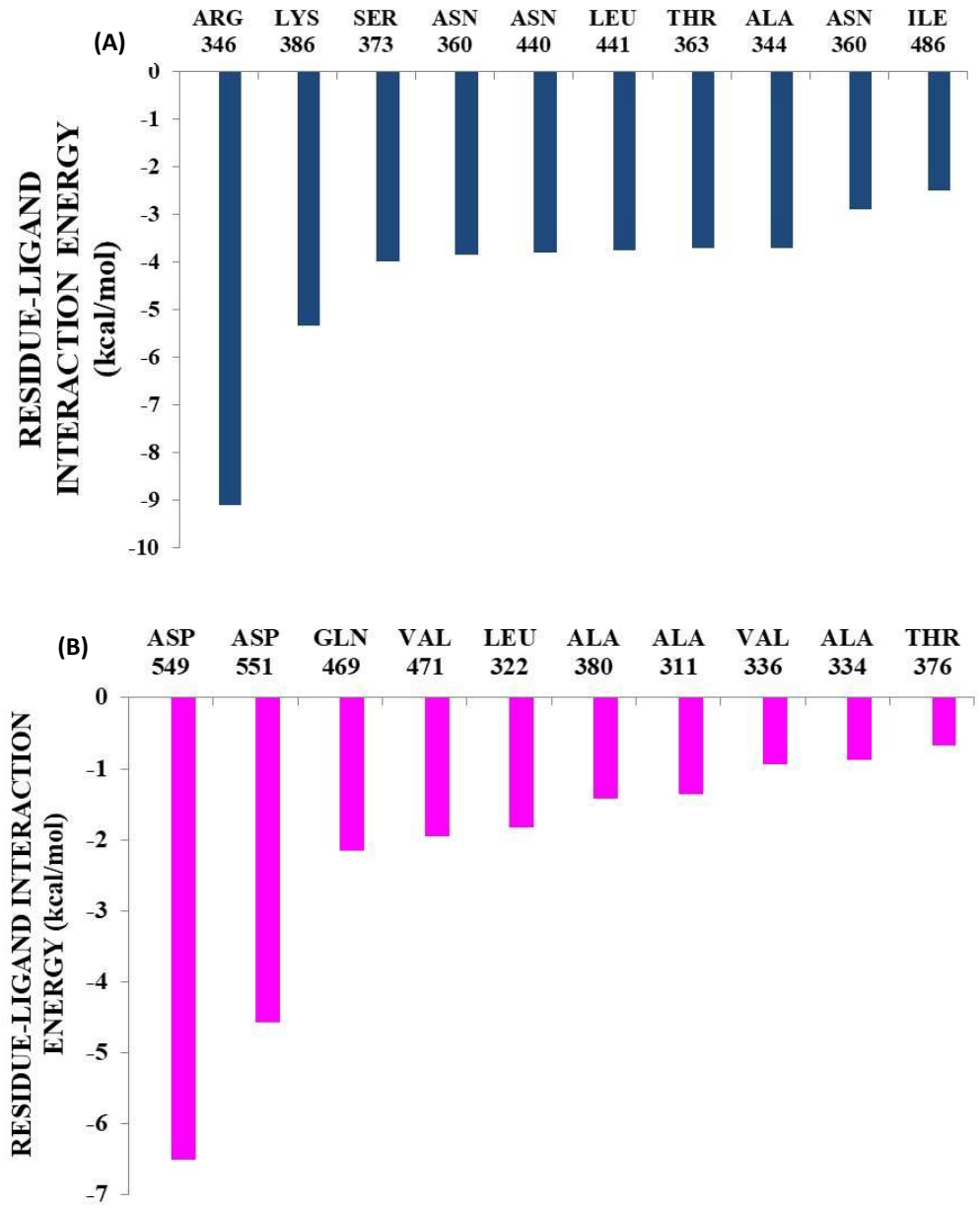

Figure 12.10. *Decomposition of binding free energy (kcal/mol) on per residue basis for* ***(A)*** *SPIKE* ***(B)*** *CAT receptor of the S protein-CAT complex.*

12.5. Conclusion:

It is difficult to say whether the S protein of SARS-CoV 2 binding to the ACE2 receptor induces a more severe form of COVID-19 illness than the binding of these recently found receptors (CAT & L-SIGN). It is unclear at this time if the S protein's interaction with receptors other than ACE2 is the root cause of the higher mortality. The current study utilizes MD simulation and other computational techniques to demonstrate the impact of SARS-CoV-2 RBD towards its binding with the CAT and L-SIGN. From the RMSD, RMSF, and a number of inter-molecular hydrogen bond analyses, we found

the S protein-CAT complex to have a greater stability when compared to the S protein-L-SIGN complex and S protein-ACE2 complex. A similar pattern was found when the number of interactions between the S protein and receptors was analyzed and it was found that the overall interactions (which included non-bonded contacts, Hydrogen bonds and salt bridges) are also higher in the S protein- CAT complex. From the binding free energy calculations of the S protein-CAT and S protein-L-SIGN complexes, we found that the affinity between S protein and CAT is higher which may infer the higher stability of the S protein-CAT complex. Higher virulence of SARS-CoV-2 may derive from the S protein-CAT complex's overall stability and greater affinity of S protein for CAT. The discovery of novel inhibitors to combat coronavirus strains that are currently on the rise may be aided by the important interaction studies between the S protein and the receptors.

12.6. Bibliography:

[1]. Mahase, E. COVID-19: WHO declares pandemic because of "alarming levels" of spread, severity, and inaction. *BMJ*, 368: m1036, 2020. http://dx.doi.org/10.1136/bmj.m1036

[2]. Senior, K. Novel human coronavirus associated with respiratory disease. *The Lancet Infectious Diseases*, 5(3): 137, 2005. http://dx.doi.org/10.1016/S1473-3099(05)70012-8

[3]. Li, J., Gong, X., Wang, Z., Chen, R., Li, T., Zeng, D., and Li, M. Clinical features of familial clustering in patients infected with 2019 novel coronavirus in Wuhan, China. *Virus research*, 286: 198043, 2020. https://doi.org/10.1016/j.virusres.2020.198043

[4]. Chen, J., Wang, R., and Wei, G. W. Review of the mechanisms of SARS-CoV-2 evolution and transmission. *arXiv*, 2011.08148v1, 2021. https://arxiv.org/abs/2011.08148

[5]. Mohan, B. S., and Vinod, N. COVID-19: An insight into SARS-CoV-2 pandemic originated at Wuhan City in Hubei Province of China. *Journal of Infectious Diseases and Epidemiology, 6*(4): 146, 2020. https://doi.org/10.23937/2474-3658/1510146

[6]. Nelson, C. W., Ardern, Z., Goldberg, T. L., Meng, C., Kuo, C. H., Ludwig, C., Kolokotronis, S. O., and Wei, X. Dynamically evolving novel overlapping gene as a factor in the SARS-CoV-2 pandemic. *eLife,* 9: e59633, 2020. https://doi.org/10.7554/eLife.59633

[7]. Heanoy, E. Z., Uzer, T., and Brown, N. R. COVID-19 pandemic as a transitional event: From the perspective of the transition theory. *Encyclopedia, 2*(3), 1602–1610, 2022. https://doi.org/10.3390/encyclopedia2030109

[8]. Guan, W., Ni, Z., Hu, Y., Liang, W., Ou, C., He, J., Liu, L., Shan, H., Lei, C., Hui, D. S. C., Du, B., Li, L., Zeng, G., Yuen, K. Y., Chen, R., Tang, C., Wang, T., Chen, P., Xiang, J., Li, S., Wang, J., Liang, Z., Peng, Y., Wei, L., Liu, Y., Hu, Y., Peng, P., Wang, J., Liu, J., Chen, Z., Li, G., Zheng, Z., Qiu, S., Luo, J., Ye, C., Zhu, S., and Zhong, N. Clinical characteristics of coronavirus disease 2019 in

China. *The New England Journal of Medicine,* 382(18): 1708–1720, 2020. https://doi.org/10.1056/NEJMoa2002032

[9]. Li, W., Moore, M. J., Vasilieva, N., Sui, J., Wong, S. K., Berne, M. A., Somasundaran, M., Sullivan, J. L., Luzuriaga, K., Greenough, T. C., Choe, H., and Farzan, M. Angiotensin-converting enzyme 2 is a functional receptor for the SARS coronavirus. *Nature*, 426(6965): 450–454. 2003. https://doi.org/10.1038/nature02145

[10]. Chakraborti, S., Prabakaran, P., Xiao, X., and Dimitrov, D. S. The SARS coronavirus S glycoprotein receptor binding domain: Fine mapping and functional characterization. *Virology Journal,* 2(1): 73, 2005. https://doi.org/10.1186/1743-422X-2-73

[11]. He, Y., Zhou, Y., Liu, S., Kou, Z., Li, W., Farzan, M., and Jiang, S. Receptor-binding domain of SARS-CoV spike protein induces highly potent neutralizing antibodies: implication for developing subunit vaccine. *Biochemical and biophysical research communications*, 324(2): 773–781, 2004. https://doi.org/10.1016/j.bbrc.2004.09.106

[12]. Mou, H., Raj, V. S., van Kuppeveld, F. J., Rottier, P. J., Haagmans, B. L., and Bosch, B. J. The receptor binding domain of the new Middle East respiratory syndrome coronavirus maps to a 231-residue region in the spike protein that efficiently elicits neutralizing antibodies. *Journal of virology*, 87(16), 9379–9383, 2013. https://doi.org/10.1128/JVI.01277-13

[13]. Tai, W., He, L., Zhang, X., Pu, J., Voronin, D., Jiang, S., Zhou, Y., and Du, L. Characterization of the receptor-binding domain (RBD) of 2019 novel coronavirus: Implication for development of RBD protein as a viral attachment inhibitor and vaccine. *Cell & Molecular Immunology,* 17: 613–620, 2020. https://doi.org/10.1038/s41423-020-0400-4

[14]. Lan, J., Ge, J., Yu, J., Shan, S., Zhou, H., Fan, S., Zhang, Q., Shi, X., Wang, Q., Zhang, L., and Wang, X. Structure of the SARS-CoV-2 spike receptor-binding domain bound to the ACE2 receptor. *Nature*, 581(7807): 215–220, 2020. https://doi.org/10.1038/s41586-020-2180-5

[15]. Premkumar, L., Segovia-Chumbez, B., Jadi, R., Martinez, D. R., Raut, R., Markmann, A., Cornaby, C., Bartelt, L., Weiss, S., Park, Y., Edwards, C. E., Weimer, E., Scherer, E. M., Rouphael, N., Edupuganti, S., Weiskopf, D., Tse, L. V., Hou, Y. J., Margolis, D., Sette, A., Collins, M.H., Schmitz, J., Baric, R.S., and de Silva, A. M. The receptor binding domain of the viral spike protein is an immunodominant and highly specific target of antibodies in SARS-CoV-2 patients. *Science immunology*, 5(48): eabc8413, 2020. https://doi.org/10.1126/sciimmunol.abc8413

[16]. Verkhivker, G. Structural and computational studies of the SARS-CoV-2 spike protein binding mechanisms with nanobodies: From structure and dynamics to avidity-driven nanobody engineering. *International Journal of Molecular Sciences,* 23(6): 2928, 2022. https://doi.org/10.3390/ijms23062928

[17]. Peng, C., Zhu, Z., Shi, Y., Wang, X., Mu, K., and Yang, Y. Computational study of the strong binding mechanism of SARS-CoV-2 spike and ACE2. *ChemRxiv*, 11877492.v2, 2020. https://doi.org/10.26434/chemrxiv.11877492.v2

[18]. Laurini, E., Marson, D., Aulic, S., Fermeglia, A., and Pricl, S. Computational mutagenesis at the SARS-CoV-2 spike protein/angiotensin-converting enzyme 2 binding interface: Comparison with experimental evidence. *ACS Nano*, 15(4): 6929–6948, 2021. https://doi.org/10.1021/acsnano.0c10833

[19]. Barton, M. I., MacGowan, S. A., Kutuzov, M. A., Dushek, O., Barton, G. J., and van der Merwe, P. A. Effects of common mutations in the SARS-CoV-2 spike RBD and its ligand, the human ACE2 receptor, on binding affinity and kinetics. *eLife*, 10*:* e70658, 2021. https://doi.org/10.7554/eLife.70658

[20]. Magazine, N., Zhang, T., Wu, Y., McGee, M. C., Veggiani, G., and Huang, W. Mutations and evolution of the SARS-CoV-2 spike protein. *Viruses,* 14(3): 640, 2022. https://doi.org/10.3390/v14030640

[21]. Qi, F., Qian, S., Zhang, S., and Zhang, Z. Single-cell RNA sequencing of 13 human tissues identifies cell types and receptors of human coronaviruses. *Biochemical and Biophysical Research Communications,* 526(1): 135–140, 2020. https://doi.org/10.1016/j.bbrc.2020.03.044

[22]. Hikmet, F., Méar, L., Edvinsson, Å., Micke, P., Uhlén, M., and Lindskog, C. The protein expression profile of ACE2 in human tissues. *Molecular Systems Biology,* 16(7): e9610, 2020. https://doi.org/10.15252/msb.20209610

[23]. Hamming, I., Timens, W., Bulthuis, M. L. C., Lely, A. T., Navis, G. J., and van Goor, H. Tissue distribution of ACE2 protein, the functional receptor for SARS coronavirus: A first step in understanding SARS pathogenesis. *The Journal of Pathology,* 203(2): 631–637, 2004. https://doi.org/10.1002/path.1570

[24]. Guo, D., Guo, R., Li, Z., Zhang, Z., Zhang, Y., Wang, X., Tang, H., and Sun, B. Cat, AGTR2, L-SIGN, and DC-SIGN are potential receptors for the entry of SARS-CoV-2 into human cells. *bioRxiv*, 07.07.451411, 2021. https://doi.org/10.1101/2021.07.07.451411

[25]. Qian, Y., Li, Y., Liu, X., Luo, J., Lu, X., and Wang, X. Evidence for the CAT gene being functionally involved in the susceptibility of COVID-19. *The FASEB Journal,* 35(4): e21384, 2021. https://doi.org/10.1096/fj.202100008

[26]. Han, D. P., Lohani, M., and Cho, M. W. Specific asparagine-linked glycosylation sites are critical for DC-SIGN- and L-SIGN-mediated severe acute respiratory syndrome coronavirus entry. *Journal of Virology,* 81(21): 12029–12039, 2007. https://doi.org/10.1128/JVI.00315-07

[27]. Chan, V. S. F., Chan, K. Y. K., Chen, Y., Poon, L. L. M., Cheung, A. N. Y., Zheng, B., Chan, K. H., Mak, W., Ngan, H. Y. S., Xu, X., Xie, Y., Su, M., Hui, P. K., Chui, Y. L., Fong, D. Y. T., Wu, A., Sham, P. C., Tam, P. K. H., Yuen, K. Y., and Leung, G. M. Homozygous L-SIGN (CLEC4M) plays

a protective role in SARS coronavirus infection. *Nature Genetics, 38*(1): 38–46, 2006. https://doi.org/10.1038/ng1698

[28]. Jeffers, S. A., Tusell, S. M., Gillim-Ross, L., Hemmila, E. M., Achenbach, J. E., Babcock, G. J., Thomas, W. D., Thackray, L. B., Young, M. D., Mason, R. J., and Ambrosino, D. M. CD209L (L-SIGN) is a receptor for severe acute respiratory syndrome coronavirus. *Proceedings of the National Academy of Sciences,* 101(44): 15748–15753, 2004. https://doi.org/10.1073/pnas.0403812101

[29]. Amraei, R., Yin, W., Napoleon, M. A., Suder, E. L., Berrigan, J., Zhao, Q., Olejnik, J., Chandler, K. B., Xia, C., Feldman, J., Hauser, B. M., Caradonna, T. M., Schmidt, A. G., Gummuluru, S., Mühlberger, E., Chitalia, V., Costello, C. E., and Rahimi, N. CD209L/L-SIGN and CD209/DC-SIGN Act as Receptors for SARS-CoV-2. *ACS central science*, 7(7): 1156–1165, 2021. https://doi.org/10.1021/acscentsci.0c01537

[30]. Berman, H. M., Westbrook, J., Feng, Z., Gilliland, G., Bhat, T. N., Weissig, H., Shindyalov, I. N., and Bourne, P. E. The Protein Data Bank. *Nucleic Acids Research*, 28(1): 235-242, 2000. http://doi.org/10.1093/nar/28.1.235

[31]. Pettersen, E. F., Goddard, T. D., Huang, C. C., Couch, G. S., Greenblatt, D. M., Meng, E. C., and Ferrin, T. E. UCSF Chimera-A visualization system for exploratory research and analysis. *Journal of Computational Chemistry*, 25(13): 1605−1612, 2004. http://doi.org/10.1002/jcc.20084

[32]. Roy, A., Kucukural, A., and Zhang, Y. I-TASSER: A unified platform for automated protein structure and function prediction. *Nature Protocols, 5*(4): 725–738, 2010. https://doi.org/10.1038/nprot.2010.5

[33]. van Zundert, G. C. P., Rodrigues, J. P. G. L. M., Trellet, M., Schmitz, C., Kastritis, P. L., Karaca, E., Melquiond, A. S. J., van Dijk, M., de Vries, S. J., and Bonvin. A. M. J. J. The HADDOCK2.2 Web Server: User-Friendly Integrative Modeling of Biomolecular Complexes. *Journal of Molecular Biology*, 428(4): 720-725, 2016. https://doi.org/10.1016/j.jmb.2015.09.014

[34]. Tian, C., Kasavajhala, K., Belfon, K. A. A., Raguette, L., Huang, H., Migues, A. N., Bickel, J., Wang, Y., Pincay, J., Wu, Q., and Simmerling, C. ff19SB: Amino-Acid-Specific Protein Backbone Parameters Trained against Quantum Mechanics Energy Surfaces in Solution. *Journal of Chemical Theory and Computation*, 16(1): 528-552, 2019. https://doi.org/10.1021/acs.jctc.9b00591

[35]. Eduardo, S. C. E., Betancourt-Conde, I., Hernandez-Campos, A., Tellez-Valencia, A., and Castillo, R. In silico hit optimization toward AKT inhibition: Fragment-based approach, molecular docking, and molecular dynamics study. *Journal of Biomolecular Structure and Dynamics,* 37(16): 4301–4311, 2019. https://doi.org/10.1080/07391102.2018.1546618

[36]. Case, D. A., Cheatham III, T. E., Darden, T., Gohlke, H., Luo, R., Merz Jr., K. M., Onufriev, A., Simmerling, C., Wang, B., and Woods, R. J. The Amber biomolecular simulation programs. *Journal of Computational Chemistry*, 26(16): 1668-1688, 2005. https://doi.org/10.1002/jcc.20290

[37]. Jorgensen, W. L., Chandrasekhar, J., Madura, J. D., Impey, R. W., and Klein, M. L. Comparison of simple potential functions for simulating liquid water. *The Journal of Chemical Physics*, 79(2): 926−935, 1983. https://doi.org/10.1063/1.445869

[38]. Yoo, S., and Xantheas, S. S. Communication: The effect of dispersion corrections on the melting temperature of liquid water. *The Journal of Chemical Physics,* 134(12): 121105, 2011. https://doi.org/10.1063/1.3573375

[39]. Salomon-Ferrer, R., Götz, A. W., Poole, D., Le Grand, S., and Walker, R. C. Routine Microsecond Molecular Dynamics Simulations with AMBER on GPUs. 2. Explicit Solvent Particle Mesh Ewald. *Journal of Chemical Theory and Computation*, 9(9): 3878-3888, 2013. https://doi.org/10.1021/ct400314y

[40]. Darden, T., York, D., and Pedersen, L. Particle mesh Ewald: An N·log(N) method for Ewald sums in large systems. *Journal of Chemical Physics*, 98: 10089, 1993. https://doi.org/10.1063/1.464397

[41]. Kräutler, V., van Gunsteren, W.F. and Hünenberger, P.H. A fast SHAKE algorithm to solve distance constraint equations for small molecules in molecular dynamics simulations. *Journal of Computational Chemistry*, 22: 501-508, 2001. https://doi.org/10.1002/1096-987X(20010415)22:5<501::AID-JCC1021>3.0.CO;2-V

[42]. Berendsen, H. J. C., Postma, J. P. M., van Gunsteren, W. F., DiNola, A., and Haak, J. R. Molecular dynamics with coupling to an external bath. *The Journal of Chemical Physics*, 81(8): 3684-3690, 1984. https://doi.org/10.1063/1.448118

[43]. Roe, D. R., and Cheatham, T. E III. PTRAJ and CPPTRAJ: Software for Processing and Analysis of Molecular Dynamics Trajectory Data. *Journal of chemical theory and computation*, *9*(7): 3084–3095, 2013. https://doi.org/10.1021/ct400341p

[44]. Laskowski, R. A., Hutchinson, E. G., Michie, A. D., Wallace, A. C., Jones, M. L., and Thornton, J. M. PDBsum: a web-based database of summaries and analyses of all PDB structures. *Trends in Biochemical Sciences*, 22(12): 488-490, 1997. https://doi.org/10.1016/s0968-0004(97)01140-7

[45]. Das, C., Das, D., and Mattaparthi, V. S. K. Effect of Mutations in the SARS-CoV-2 Spike RBD Region of Delta and Delta-Plus Variants on its Interaction with ACE2 Receptor Protein. *Letters in Applied NanoBioScience*, 12(4): 118, 2023. https://doi.org/10.33263/LIANBS124.118

[46]. Das, C., Das, D., and Mattaparthi, V. S. K. Computational Investigation on the Efficiency of Small Molecule Inhibitors Identified from Indian Spices against SARS-CoV-2 Mpro. *Biointerface Research in Applied Chemistry*, 13(3): 235, 2023. https://doi.org/10.33263/BRIAC133.235

[47]. Das, C., and Mattaparthi, V. S. K. Impact of Mutations in the SARS-CoV-2 Spike RBD Region of BA1 and BA2 Variants on its Interaction with ACE2 Receptor Protein. *Biointerface Research in Applied Chemistry*, 13(4): 358, 2023. https://doi.org/10.33263/BRIAC134.358

[48]. Weng, G., Wang, E., Wang, Z., Liu, H., Zhu, F., Li, D., and Hou, T. HawkDock: a web server to predict and analyze the protein-protein complex based on computational docking and MM/GBSA. *Nucleic acids research*, *47*(W1): W322–W330, 2019. https://doi.org/10.1093/nar/gkz397

[49]. Zhang, W., Yang, F., Ou, D., Lin, G., Huang, A., Liu, N., and Li, P. Prediction, docking study, and molecular simulation of 3D DNA aptamers to their targets of endocrine-disrupting chemicals. *Journal of Biomolecular Structure and Dynamics,* 37(16): 4274–4282, 2019. https://doi.org/10.1080/07391102.2018.1547222

[50]. Gao, J., Wang,Y., Chen, Q., and Yao, R. Integrating molecular dynamics simulation and molecular mechanics/generalized Born surface area calculation into pharmacophore modeling: a case study on the proviral integration site for Moloney murine leukemia virus (Pim)-1 kinase inhibitors. *Journal of Biomolecular Structure and Dynamics*, 38(2): 581-588, 2020. https://doi.org/10.1080/07391102.2019.1571946

[51]. Das, C., Hazarika, P. J., Deb, A., Joshi, P., Das, D., and Mattaparthi, V. S. K. Effect of Double Mutation (L452R and E484Q) in RBD of Spike Protein on its Interaction with ACE2 Receptor Protein. *Biointerface Research in Applied Chemistry*, 13(1): 97, 2023. https://doi.org/10.33263/BRIAC131.097